5-*N*-Methylated Quindoline Derivatives as Telomeric G-Quadruplex Stabilizing Ligands: Effects of 5-*N* Positive Charge on Quadruplex Binding Affinity and Cell Proliferation

Yu-Jing Lu,[†,‡] Tian-Miao Ou,[†,‡] Jia-Heng Tan,[‡] Jin-Qiang Hou,[‡] Wei-Yan Shao,[‡] Dan Peng,[‡] Ning Sun,[‡] Xiao-Dong Wang,[‡] Wei-Bin Wu,[‡] Xian-Zhang Bu,[‡] Zhi-Shu Huang,[‡,*] Dik-Lung Ma,[§] Kwok-Yin Wong,[§] and Lian-Quan Gu[‡,*]

School of Pharmaceutical Sciences, Sun Yat-sen University, Guangzhou 510080, People's Republic of China, Department of Applied Biology and Chemical Technology and the Central Laboratory of the Institute of Molecular Technology for Drug Discovery and Synthesis, and The Hong Kong Polytechnic University, Hung Hom, Kowloon, Hong Kong, China, People's Republic of China

Received April 30, 2008

A series of 5-*N*-methyl quindoline (cryptolepine) derivatives (**2a**−**x**) as telomeric quadruplex ligands was synthesized and evaluated. The designed ligands possess a positive charge at the 5-*N* position of the aromatic quindoline scaffold. The quadruplex binding of these compounds was evaluated by circular dichroism (CD) spectroscopy, fluorescence resonance energy transfer (FRET) melting assay, polymerase chain reaction (PCR) stop assay, nuclear magnetic resonance (NMR), and molecular modeling studies. Introduction of a positive charge not only significantly improved the binding ability but also induced the selectivity toward antiparallel quadruplex, whereas the nonmethylated derivatives tended to stabilize hybrid-type quadruplexes. NMR and molecular modeling studies revealed that the ligands stacked on the external G-quartets and the positively charged 5-*N* atom could contribute to the stabilizing ability. Long-term exposure of human cancer cells to **2r** showed a remarkable cessation in population growth and cellular senescence phenotype and accompanied by a shortening of the telomere length.

1. Introduction

Telomeres are DNA−protein assemblies that cap the end of linear chromosomes. Their function is to protect the termini of chromosomes from recombination, end-to-end fusion, and degradation. Telomere shortening occurs progressively during cell divisions. When telomeres reach a critical short size, cells enter a stage of senescence replication, followed by cell crisis and apoptosis. Human telomere is composed of random repeats of guanine-rich sequence d[$(TTAGGG)_n$].[1−3] The telomerase overexpressed in most tumor cells is a RNA-dependent DNA polymerase that uses its endogenous RNA template to catalyze the elongation of telomere, thus maintaining the telomere length and rendering the tumor cells with an almost infinite capacity to divide and to be immortal.[4−8] This unique telomerase activity and telomere capping function are becoming powerful and promising targets for cancer chemotherapy.[9−15]

In addition to targeting the enzyme itself, an alternative approach is to stabilize higher-order quadruplex structures formed by G-rich sequence d[$(TTAGGG)_n$], which is used by telomerase as a primer during the elongation phase.[16] In vitro, a number of small molecule ligands have been identified to stabilize G-quadruplex structures and inhibit telomerase activity. These include the natural product telomestatin,[17] cationic porphyrins,[18] substituted acridines,[19−21] polycyclic aceidines,[22] and perylenetetracarboxylic diimide derivatives.[23,24] Furthermore, in cellular experiments, several classes of these compounds have been shown to have pronounced effects on cancer cell lines, suggesting that the postulated action mechanism of these compounds is a denial of telomerase access to the telomere.[25−28]

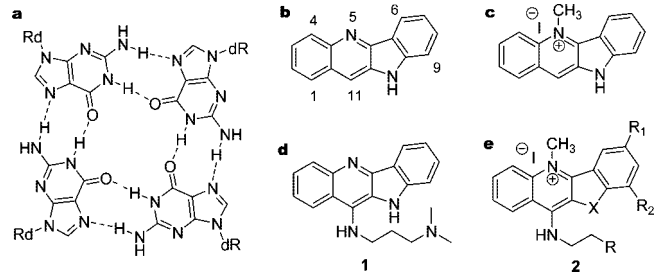

Figure 1. Structures of the G-quartet (a), quindoline (b), cryptolepine (c, salt form), **1** (d), and 11-alkylamines substituted 5-*N*-methyl quindoline derivatives (e).

Quindoline and cryptolepine (Figure 1b,c) belong to the indoloquinoline family, a relatively rare group of alkaloids in nature.[29] Cryptolepine and its hydrochloride salt possess interesting biological properties and have been used as antimalarial drugs in Central and Western Africa for centuries.[30,31] Further mechanistic investigation at the molecular level demonstrated that cryptolepine could interact with DNA through intercalation.[32] Most recent studies further revealed that some structural derivatives of quindoline were capable of interacting with the telomeric G-quadruplex structure and showed inhibitory effect on telomerase.[33−35] Quindoline derivative **1** (SYUIQ-5, Figure 1d) had been developed by us as the quadruplex stabilizing ligand and potent telomerase inhibitor.[36,37] Subsequent studies on this ligand indicated that the 11-alkylamino group on quindoline could provide the in situ protonation ability of the 5-*N* atom. Molecular modeling studies on the binding mode of these quindolines with quadruplex revealed that the crescent aromatic core stacked on two guanine residues of the G-quartet and the 5-*N* electropositive center overlapped with the cation channel of the quadruplex, thereby achieving effective stabilization and selective recognition of G-quadruplex. However, the

* To whom correspondence should be addressed. Phone: 8620-39332679 (Z.-S.H.); 8620-39332678 (L.-Q.G.). Fax: 8620-39332678 (Z.-S.H. and L.-Q.G.). E-mail: ceshzs@mail.sysu.edu.cn (Z.-S.H.); cesglq@mail.sysu.edu.cn (L.-Q.G.).

† These authors contributed equally to this paper.

‡ School of Pharmaceutical Sciences, Sun Yat-sen University, Guangzhou 510080, China.

§ Department of Applied Biology and Chemical Technology and the Central Laboratory of the Institute of Molecular Technology for Drug Discovery and Synthesis, The Hong Kong Polytechnic University, Hung Hom, Kowloon, Hong Kong, China.

10.1021/jm800497p CCC: $40.75
Published on Web 09/27/2008

Scheme 1. Synthesis of 5-*N*-Methyl Quindoline Derivative[a]

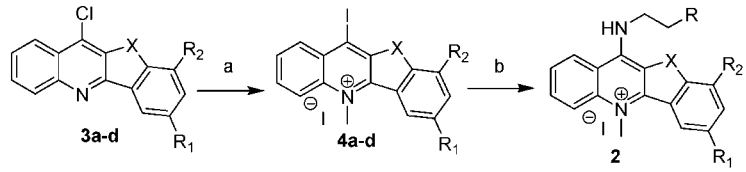

2a X = NH, R_1=R_2=H, R = $N(CH_3)_2$	**2i** X = O, R_1=R_2=H, R = $N(CH_3)_2$	**2q** X = NH, R_1=F, R_2=H, R = $N(CH_3)_2$
2b X = NH, R_1=R_2=H, R = $CH_2N(CH_3)_2$	**2j** X = O, R_1=R_2=H, R = $CH_2N(CH_3)_2$	**2r** X = NH, R_1=F, R_2=H, R = $CH_2N(CH_3)_2$
2c X = NH, R_1=R_2=H, R = $N(C_2H_5)_2$	**2k** X = O, R_1=R_2=H, R = $N(C_2H_5)_2$	**2s** X = NH, R_1=F, R_2=H, R = $N(C_2H_5)_2$
2d X = NH, R_1=R_2=H, R = $CH_2N(C_2H_5)_2$	**2l** X = O, R_1=R_2=H, R = $CH_2N(C_2H_5)_2$	**2t** X = NH, R_1=F, R_2=H, R = $CH_2N(C_2H_5)_2$
2e X = NH, R_1−R_2−H, R − morphoryl	**2m** X = O, R_1−R_2−H, R − morphoryl	**2u** X = NH, R_1−F, R_2−F, R − $N(CH_3)_2$
2f X = NH, R_1=R_2=H, R = methylmorpholine	**2n** X = O, R_1=R_2=H, R = methylmorpholine	**2v** X = NH, R_1=F, R_2=F, R = $CH_2N(CH_3)_2$
2g X = NH, R_1=R_2=H, R = OH	**2o** X = O, R_1=R_2=H, R = OH	**2w** X = NH, R_1=F, R_2=F, R = $N(C_2H_5)_2$
2h X − NH, R_1−R_2−H, R − CH_2OH	**2p** X − O, R_1−R_2−H, R − CH_2OH	**2x** X − NH, R_1−F, R_2−F, R − $CH_2N(C_2H_5)_2$

[a] Reaction conditions: (a) CH_3I, sulpholane, 55 °C, overnight; (b) substituted alkylamine, 2-ethoxyethanol, 120 °C, 30 min.

pK_a values of the 5-*N* atom of 11-aminoquindolines were 8.2−8.4[36] and thus could be influenced easily by the solution condition. Besides the introduction of the positive charge via in situ protonation, an alternative pathway was *N*-methylation at 5-position.[38] The advantage of this design was multiple, including introduction of a steady positive charge for the electrostatic interaction and increasing π-stacking interaction due to the reduction of the electron density of the aromatic core of ligand. On this basis, a series of 5-*N*-methyl quindoline (cryptolepine) derivatives were designed for screening the ligands with better binding ability and selective recognition of G-quadruplex. We reported here our biophysical, biochemical, and cellular evaluation studies on the binding of the 5-*N*-methyl quindoline derivatives to telomeric quadruplex DNA and its relationship with telomere biological functions. CD data revealed that the 5-*N*-methyl quindoline derivatives selectively induced the formation of the antiparallel G-quadruplex in K^+ solution, whereas the nonmethylated quindoline derivatives could only induce hybrid-type quadruplexes (Supporting Information). All the results revealed that the introduction of a positive charge by methylation at the 5-*N* position of 11-aminoquindoline significantly improved the binding ability and inhibitory effect on the telomere biological functions. To investigate how changes in electronic distribution on the skeleton of the ligand could modify its ability to stack onto the G-quadruplex, one or more fluorine substituents were introduced on some of 5-*N*-methyl quindoline derivatives. In addition, NMR and molecular modeling studies were used to investigate the structure−activity relationships and to probe the binding modes.

2. Results and Discussion

2.1. Chemistry. The key intermediates of 11-chloroquindoline **3** was prepared following the procedure reported by Bierer et al.[30] The selective *N*-5 methylation of 11-chloroquindoline with iodomethane was achieved in the presence of sulfolane with an excellent yield (88−93%). Sulpholane was reported as a solvent for certain *N*-quarternization reactions that were used for selective *N*-alkylation of quindoline.[39] The substitution reaction of compounds **4** with various alkylamines gave the final products of 11-amino 5-*N*-methyl quindoline derivatives **2a**−**2x** (Scheme 1). All the substitution reactions were completed in high yields (80−92%) within 30 min.

2.2. Converting the Preformed Hybrid-Type G-Quadruplex to the Antiparallel G-Quadruplex by 5-*N*-Methyl Quindoline Derivatives in the Presence of K^+. Circular dichroism (CD) spectroscopy was employed to determine the formation of G-quadruplex in the presence of 5-*N*-methyl quindoline derivatives. It had been reported that the human telomeric sequence d[$G_3(T_2AG_3)_3$] (HTG21) formed a typical antiparallel quadruplex DNA structure in the presence of Na^+, with a large positive band at 295 nm and a negative band at 265 nm in CD spectra. On the other hand, the CD spectra of HTG21 in the presence of K^+ exhibited a large positive band at 290 nm, a small positive band at 270 nm, and a negative band at 235 nm, which suggested that HTG21 might exist as a hybrid-type of quadruplex DNA containing parallel and antiparallel structure.[40−43] Upon addition of compound **2b** to HTG21 in buffer containing K^+, the CD spectra changed with a disappearance of the small positive band at 270 nm, indicating the possible destruction of the parallel structure of the mixed G-quadruplex conformations, while the positive band at about 290 nm increased obviously and the negative band at about 260 nm appeared, suggesting the formation of an antiparallel structure (Figure 2A). CD studies in sodium solution were also carried out to examine the effects of compounds on different G-quadruplex structures, although they were less physiologically relevant. However, upon addition of **2b** to HTG21 in buffer containing Na^+, the CD spectra changed only slightly with a small increase at about 290 nm (Supporting Information). The other derivatives induced similar CD changes under the same conditions (Supporting Information). Results from these CD experiments suggest that 5-*N*-methyl quindoline derivatives could convert the preformed hybrid-type G-quadruplex structure into antiparallel G-quadruplex. Also, the stoichiometry of the binding of 5-*N*-methyl quindoline derivative to G-quadruplex was determined from CD spectra. When **2b** was titrated against the HTG21 in the presence of K^+, the band at 290 nm gradually increased until a ratio of **2b** to HTG21 equal to 2:1 was reached. The changes at 290 nm as a function of **2b**/HTG21 (*r*) were plotted in Figure 2B, and the curve was fitted to an exponential function that suggested the formation of a 2:1 **2b**−HTG21 complex.

2.3. Thermodynamic Stability of the Telomeric G-Quadruplex by 5-*N*-Methyl Quindoline Derivatives. Thermodynamic stability of 5-*N*-methyl quindoline derivatives to the G-quadruplex DNA was determined from the melting temperature of the G-quadruplex DNA incubated with 5-*N*-methyl quindoline derivatives using a fluorescence resonance energy transfer (FRET) assay.[44,45] All melting temperature assays were carried out in triplicate, and the quindoline derivative **1**[36,37] previously reported by us (Figure 1d) was used as a reference compound. It was known that **1** caused a rise of the melting

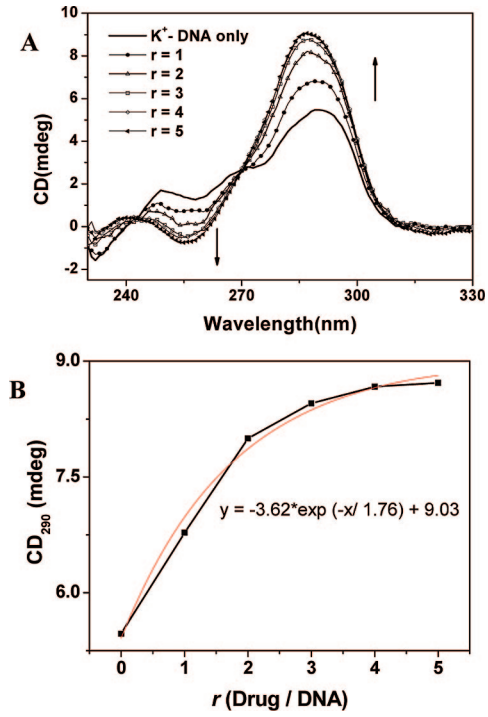

Figure 2. (A) CD titration spectra of HTG21 in the presence of various concentrations of **2b** in Tris-HCl buffer containing KCl. (B) Curve representing the changes in CD titration spectra was fitted to an exponential function and a 2:1 stoichiometry was assigned from the function. All spectra were collected in a strand concentration of 5 μM in 10 mM Tris-HCl buffer (pH 7.4).

Table 1. G-Quadruplex FRET and PCR Stop Assay Data by **1** and **2a**−**x**[a]

compd	ΔT_m/°C	IC_{50}/μM	compd	ΔT_m/°C	IC_{50}/μM	compd	ΔT_m/°C	IC_{50}/μM
2a	13	10.3	**2i**	11	11.5	**2q**	14	13
2b	17	4.5	**2j**	14	6.1	**2r**	14	8
2c	12	12	**2k**	12	13	**2s**	12	18
2d	19	5.1	**2l**	15	5.7	**2t**	18	5
2e	10	>20	**2m**	9	>20	**2u**	11	>20
2f	12	>20	**2n**	13	18	**2v**	15	9
2g	5	>20	**2o**	4	>20	**2w**	11	15
2h	7	>20	**2p**	10	>20	**2x**	15	5.5
1	9	>20						

[a] The melting point of native DNA quadruplex was 60 °C. ΔT_m, change in melting temperature at 1 μM compound concentration and 200 nM DNA concentration; IC_{50}, concentration of compound required to achieve 50% inhibition of PCR.

temperature of the native quadruplex DNA in 60 mM potassium from 60 to 69 °C.

The effects of compounds **2a**−**2x** on the T_m of the G-quadruplex are summarized in Table 1. A comparison of the FRET assay results for the reference compound **1** and **2b** (both with the same side chain substituent) revealed that introduction of the positive charge by methylation at the 5-*N* position of quindoline significantly improved the stability of the quadruplex structure. Previous reports on nonmethylated quindoline derivatives[36] indicated that derivatives with a pyrrole ring in the aromatic core showed a comparatively higher T_m value than those with a furan ring. However, a similar trend was not observed in the 5-*N*-methyl quindoline derivatives. This suggested that the effects of pyrrole ring or furan ring in the aromatic core on the electron density were limited when a positive charge of 5-*N* position presented in the quindoline skeleton. Similarly, to study whether changes in the electronic distribution of the core could influence the binding ability of the ligand with the G-quadruplex, a fluorine substituent was introduced in **2q**−**2x**. The electron-withdrawing effect of the fluorine could further reduce the electron density of the skeleton, which might favor a stronger interaction with the electron-rich π-system of the G-quartet. However, the introduction of the fluorine did not show an obvious effect either on quadruplex binding or biological activity. Nevertheless, the attachment of weakly basic groups (e.g., hydroxyl) to the side chain could decrease the binding affinity with G-quadruplex DNA, suggesting that electrostatic interaction between the ligand side chain and the G-quadruplex structure was an important factor for the recognition process.

2.4. Inhibition of Amplification in HTG21 by 5-*N*-Methyl Quindoline Derivatives. To further evaluate the ability of 5-*N*-methyl quindoline derivatives to stabilize G-quadruplex DNA, polymerase chain reaction (PCR) stop assay was carried out. In the presence of 5-*N*-methyl quindoline derivatives, the template sequence HTG21 was induced into a G-quadruplex structure that blocked the hybridization with a complementary primer sequence. In that case, 5′ to 3′ primer extension by DNA *Taq* polymerase was arrested and the final double-stranded DNA PCR product could not be detected.[46,47] Concentrations of derivatives **2a**−**x** and **1** that inhibited amplification by 50% (IC_{50}) are listed in Table 1. A correlation between the PCR stop assay results and FRET data could be drawn, and derivatives with greater stabilizing power of G-quadruplex structure were in general better inhibitors of amplification in HTG21. Compounds **2b**, **2d**, **2j**, **2l**, **2t**, and **2x**, with dimethylpropane-1,3-diamine or diethylpropane-1,3-diamine side chain, were most effective in these aspects.

2.5. Binding Mode between 5-*N*-Methyl Quindoline Derivatives and G-Quadruplex. To further investigate the binding affinity and binding modes between the 5-*N*-methyl quindoline derivatives and G-quadruplex structures, nuclear magnetic resonance (NMR) studies and molecular modeling studies were performed.[23] NMR titration experiments clearly showed a 2:1 stoichiometry for binding of ligand **2r** to the intermolecular four-stranded parallel quadruplex [$d(T_2AG_3)$] derived from human telomeric DNA sequences (Supporting Information). The more pronounced change of the G4 and G6 imino proton inferred that the ligand stacks over 3′- and 5′-G-quartet. The thermal denaturation behavior of the G-quadruplex in the absence and presence of ligand **2r** revealed that the interaction of ligand **2r** increased the T_m by about 25 °C (Supporting Information).

Molecular docking studies were performed on some of G-quadruplex-ligand complexes to investigate the best binding mode between the G-quadruplex and the 5-*N*-methylated quindoline derivatives. The crystal structure of the propeller telomeric G-quadruplex ($d[AG_3(T_2AG_3)_3]$, PDB code: 1KF1[48]) with potassium was used as the starting point for the modeling because it might be the more biologically relevant form.[49] This G-quadruplex structure could be characterized by two external G-quartet planes. The 5′ G-quartet surface was relatively more hydrophobic for favoring $\pi-\pi$ stacking interactions, whereas the 3′ G-quartet surface was more favored for electronic interactions (Supporting Information). Our study showed that 5-*N*-methylated quindoline derivatives could stack on both external G-quartet planes. However, results from clustering analysis of molecular docking indicated that in most cases derivatives prefer to stack on the 3′ G-quartet plane (Supporting Information). The docking results also showed the terminal protonated amino group could interact with phosphate diester backbone by electrostatic interaction and hydrogen bond. The

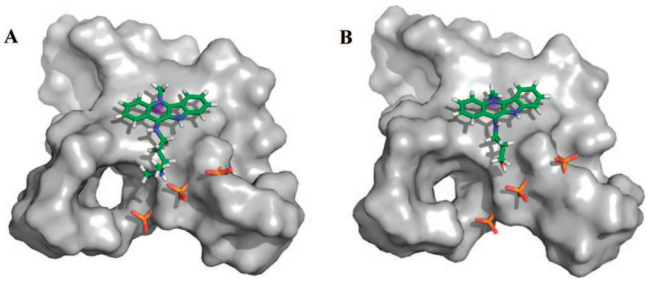

Figure 3. View onto the plane of the 3′ surface of human G-quadruplex complex with compound **2b** (A) and **2h** (B), showing the interaction between compound and G-quadruplex. Picture was created with PyMOL.

Table 2. Estimated Free Energy of Binding in MM-GBSA Calculations

compd	ΔG/kcal·mol^{-1}	compd	ΔG/kcal·mol^{-1}
2a	−18.2	**2j**	−26.38
2b	−25.35	**2l**	−23.34
2c	−17.57	**2r**	−18.76
2d	−29.81	**2t**	−28.47
2f	−20.89	**2v**	−21.24
2h	−15.61	**2x**	−19.56
1	−13.21		

complexes obtained from docking studies were used for subsequent molecular dynamics studies.

The MD runs for the complexes showed that the crescent-like quindoline skeleton could interact with at least two guanines, thus stabilized the G-quadruplex. The methylation on the 5-*N* atom of quindoline could significantly increase the electrostatic interaction between the positively charged center of the quindoline skeleton and the negatively charged carbonyl channel of G-quadruplex. The terminal protonated amino group tended to interact with phosphodiester backbone by electrostatic interaction and hydrogen bonds. Compounds with a hydroxyl end could also interact with phosphodiester backbone by forming hydrogen bonds but much weaker than those with terminal amino group (Figure 3). Elongation of the side chains by one methylene caused the protonated amino group in the side chain to reach the phosphodiester backbone, accompanied by a correspondingly increased binding affinity. Compounds **2b**, **2d**, **2j**, and **2t**, with dimethylpropane-1,3-diamine or diethylpropane-1,3-diamine side chain, possessed the most favorable interaction (lower binding free energy). These results approximately parallel the trend in the FRET assay data and PCR stop assay data. The correlation between FRET assay results and the MM-GBSA-calculated binding energy (Table 2) had been explored in Figure 4, and the correlation coefficient was 0.75.

2.6. Competition Dialysis Assay. Competition dialysis assay was used to evaluate the selectivity of 5-*N*-methyl quindoline derivatives toward various G-quadruplex and other DNA structures. In this assay, the various nucleic acids were dialyzed simultaneously against a free ligand solution. Higher binding affinity was reflected by the higher concentration of ligands accumulated in the dialysis tube containing the specific form of DNA.[50] The various forms of DNA used in the assay include HTG21 and Pu27 [d($TG_4AG_3TG_4AG_3TG_4A_2G_2$)], which form the intramolecular G-quadruplex structures, HT-7 [d(T_2AG_3T)], the intermolecular G-quadruplex structure, HTC21 [d($C_3[TA_2C_3]_3$)], the i-motif structure, $(dT21)_2$/dA21, which associate to give a triplex structure, dT21/dA21, a duplex structure, HTds, a 21-mer duplex structure (from human telomere sequence), HTG21mu [d(GAG[T_2AGAG]$_3$)], a single-strand structure (a mutant oligomer of human telomere sequence containing multiple mutant sites), and dA21 and dT21, which

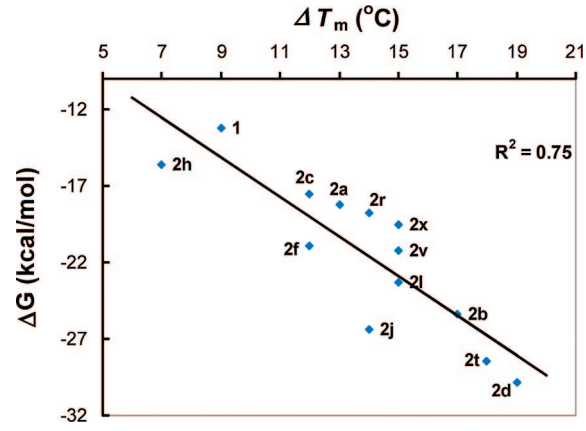

Figure 4. Plots of Calculated Binding Energies vs FRET Assay Data.

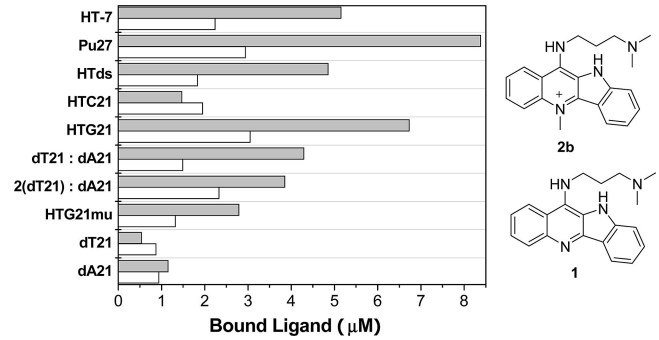

Figure 5. Results of competition dialysis assay. A 1 μM solution of **1** or **2b** was dialyzed against 10 different nucleic acid structures (45 μM) for 24 h. The amount of bound ligand, **1** (white) or **2b** (gray), was plotted against each DNA structure as a bar.

were single-strands of purine and pyridine respectively. The data on the amount of the ligands bound to the 10 structurally different nucleic acids, which should be proportional to the binding affinity for each conformational form of DNA, are shown in Figure 5.

As shown in Figure 5, 5-*N*-methyl quindoline derivative **2b** displayed stronger binding to different types of DNA than the quindoline derivative **1**, especially for G-quadruplexes. Compound **2b** interacted preferentially with the G-quadruplex DNA of Pu27 and HTG21, while little binding to single strands was observed. The binding affinities for double strands and triplex were lower than those for quadruplexes. Overall, these studies indicated that **2b** binds preferentially to the quadruplexes and had a better selectivity for G-quadruplex DNA than **1**.

2.7. Inhibition of Telomerase Activity in Cell-Free System. The contribution of the positive charge by methylation on the quindoline for telomerase inhibition was investigated using telomerase repeat amplification protocol (TRAP) assay.[51] Although the limitation of TRAP was reported recently,[52] the data from this experiment could be used to make the comparison between different quindoline ligands. In this experiment, solutions of quindoline derivatives at certain concentrations were added to the telomerase reaction mixture containing extract from cracked MCF-7 breast carcinoma cell lines and the inhibitory concentrations by half ($^{Tel}IC_{50}$) values of these compounds are listed in Table 3. It was found that the inhibitory effects on telomerase activity of 5-*N*-methyl quindoline derivatives were significantly enhanced when compared to the quindoline derivative **1**. Thus introducing a positive charge by methylation on the 5-*N* of quindoline could improve its inhibitory ability

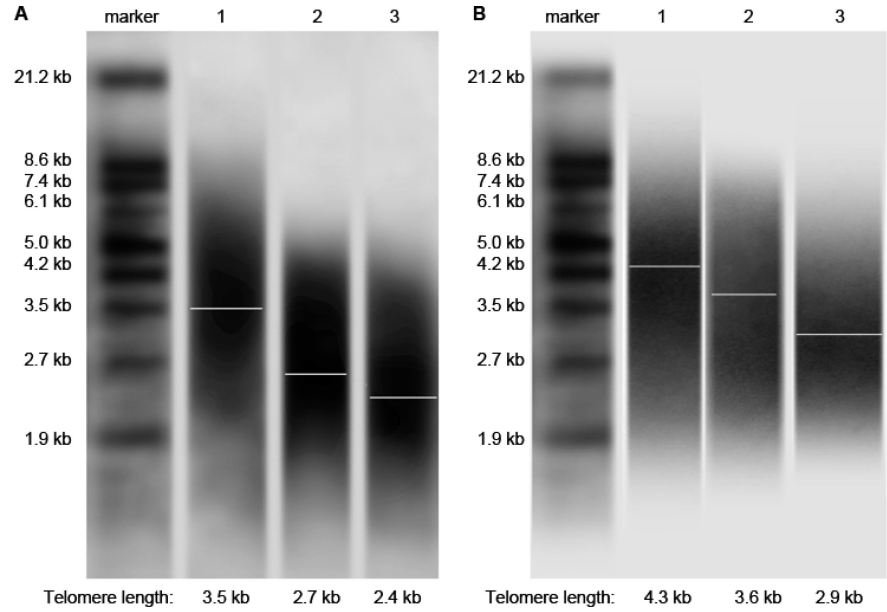

Figure 6. Effect of quindoline derivative **2r** on telomere length. TRF of cancer cells treated or untreated with **2r** was analyzed using the *T*elo *TAGGG* telomere length assay. (A) TRF analysis of HL60 cells treated or untreated with **2r** for 16 days. Lane 1, 0.1% DMSO; lane 2, 0.03 μM **2r**; lane 3, 0.06 μM **2r**. (B) TRF analysis of CA46 cells treated or untreated with **2r** for 16 days. Lane 1, 0.1% DMSO; lane 2, 0.03 μM **2r**; lane 3, 0.06 μM **2r**.

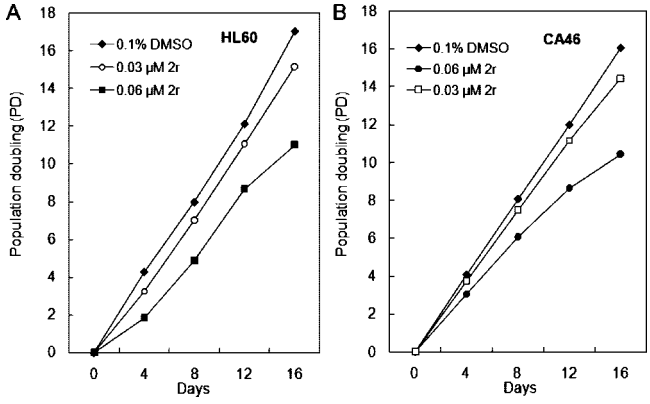

Figure 7. Long-term exposure of HL60 (A) and CA46 cells (B) with **2r** at subcytotoxic concentrations. Cells were exposed to indicated concentrations of **2r** or 0.1% DMSO, respectively. Every 4 days, the cells in control and drug-exposed flasks were counted and flasks reseeded with cells. Each experiment was performed three times at each point. This experiment was a representative of three experiments.

Table 3. Telomerase Inhibition by **1** and 5-*N*-Methyl Quindolines in Cell-Free Assay

	1	**2b**	**2d**	**2j**	**2r**	**2t**	**2v**	**2x**
$^{Tel}IC_{50}$ (μM)	0.63	0.22	0.16	0.37	0.31	0.20	0.40	0.27

against telomerase. These results were in line with the current thinking that a stronger ligand of the G-quadruplex was also a good inhibitor of telomerase activity. In this way, 5-*N*-methyl quindoline derivatives might act as a "pseudo-potassium ion", which could induce the formation and stabilization of the G-quadruplex and thus exhibited a strong inhibitory effect on telomerase activity.

2.8. Shortening of the Telomere Length by 2r. Inhibition of telomerase and interaction with telomere G-overhang in cancer cells was predicted to disrupt telomere length maintenance and caused telomeres to erode. To investigate whether **2r** could cause telomeres to shorten, the telomere length was evaluated using the telomeric restriction fragment (TRF) length assay. The results showed that 0.06 μM of **2r** triggered telomere shortening about 1.1 kb against HL60 cells, and telomere shortening was also observed after 0.03 μM of **2r** treatment (Figure 6A). Similar reduction in telomere length was observed in CA46 cells; 0.06 μM of **2r** caused telomere shortening of about 1.4 kb against CA46 cells (Figure 6B). The results indicated that the derivative **2r** could inhibit the elongation of telomeres in two cell lines of HL60 and CA46, although the real action mechanism of this inhibition needed to further study.

2.9. Senescence Induced by 5-*N*-Methyl Quindoline Derivative 2r. To examine the effect of ligand **2r** on leukemia cell HL60 and lymphoma cell CA46, short-term cell viability was determined in a two-day cytotoxic assay (MTT assay) first. Results showed that **2r** had a potent inhibitory effect with an IC_{50} value of 1.21 μM in HL60 and 1.36 μM in CA46.

To avoid acute cytotoxicity and other nonspecific events that could lead to difficulty in result interpretation, subcytotoxic concentrations (0.03 and 0.06 μM) of **2r** were evaluated on HL60 and CA46 cells for long-term exposure. Treatment of HL60 cells with 0.06 μM **2r** resulted in an arrest in cell growth at day 12, and even with 0.03 μM **2r**, the population doubling time increased substantially compared to the control (Figure 7A). The similar results were observed in another human lymphoma cell line CA46 cells. Morphologic examination of the cells at the plateau phase displayed an increased proportion of flat and giant cells with phenotypic characteristics of senescence[53,54] as revealed by the senescence-associated β-galactosidase (SA-β-Gal) assay method (Figure 8). For dysfunctional telomeres that could activate p53 to initiate cellular senescence or apoptosis to suppress tumorigenesis, this effect of **2r** to induce senescence might result from the shortening effect to telomere length.

3. Conclusions

A series of 5-*N*-methyl quindoline (cryptolepine) derivatives (**2a**−**x**) as telomeric quadruplex stabilizing ligands have synthesized and evaluated by CD spectroscopy, FRET-melting assay, PCR stop assay, NMR study, molecular modeling, competition dialysis assay, inhibitory telomerase activity test,

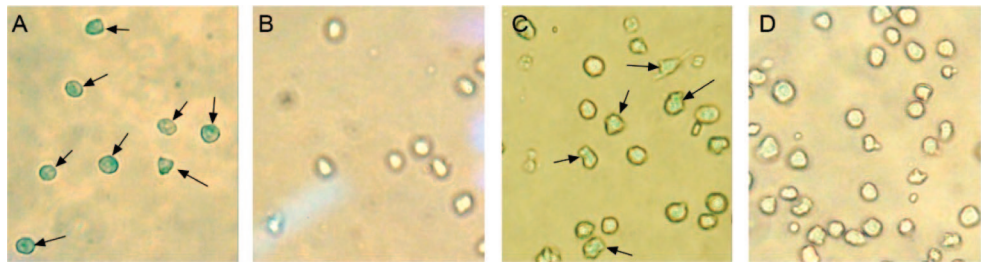

Figure 8. Expression of SA-β-Gal in HL60 and CA46 cells after continuous treatment with **2r**. HL60 cells were treated with 0.06 μM **2r** (A) or 0.1% DMSO (B) continuously for 16 days. CA46 cells were also treated with 0.06 μM **2r** (C) or 0.1% DMSO (D) continuously for 16 days. Then, cells were fixed, stained with SA-β-Gal staining kit, and photographed (×400). This experiment was repeated twice.

and series cellular studies. All of the results clearly showed that these ligands were capable of inducing the formation of antiparallel G-quadruplex in the presence of K^+. NMR study and molecular modeling revealed the binding mode was external-stacking on the G-tetrad, and the positively charged 5-*N* position of quindoline core could contribute to the overall stabilizing ability. Treatment with the ligand **2r** remarkably inhibited the telomerase activity in a cell-free system. Long-term exposure assays of HL60 leukemia cells and CA46 lymphomas cells showed ligand **2r** could induce a remarkable cessation in population growth, cellular senescence phenotype, and shortening of telomere length.

4. Experimental Section

Synthesis and Characterization. Melting points were recorded on a Leica Galen III hot-stage melting point apparatus and were uncorrected. ^{1}H NMR spectra were recorded on a 300 MHz Mercury-Plus spectrometer using TMS as an internal standard in DMSO-d_6, $CDCl_3$, or CD_3OD. ^{13}C NMR spectra were recorded on a Varian Unity 400 NMR instrument at 100 MHz. Mass spectra were recorded on a VG ZAB-HS (fast atom bombardment) spectrometer. High-resolution mass spectra were obtained with a MAT95XP (Thermo) mass spectrometer. Elemental analyses were carried out on an Elementar Vario EL CHNS elemental analyzer. All compounds were routinely checked by TLC with Merck silica gel 60F-254 glass plates. 11-Chloroquindoline **3a**−**d** was synthesized as reported.[30] Analytical data for compound 11-chloro-10*H*-indolo[3,2-*b*]quinoline (**3a**) and 11-chlorobenzofuro[3,2-b]- quinoline (**3b**) have been previously presented.[36]

11-Chloro-7-fluoro-10*H*-indolo[3,2-*b*]quinoline (11-Chloro-7-fluoro-quindoline) (3c). Compound **3c** was synthesized by a literature procedure;[30] mp 207−209 °C. ^{1}H NMR (300 MHz, $CDCl_3$): δ 11.86 (s, 1H), 8.26 (m, 2H), 8.10(d, J = 8.4 Hz, 1H), 7.75 (m, 2H), 7.61 (m, 1H), 7.53 (t, J = 9.0 Hz, 1H). FAB-MS m/z: 271 $[M + 1]^+$. Anal. ($C_{15}H_8ClFN_2$) C, H, N.

11-Chloro-7,9-difluoro-10*H*-indolo[3,2-*b*]quinoline (11-Chloro-7,9-difluoro-quindoline) (3d). Compound 3d was synthesized by a literature procedure;[30] mp 204−206 °C. ^{1}H NMR (DMSO-d_6, 300 Hz): δ 12.22 (s, 1H), 8.21 (t, J = 7.2 Hz, 2H), 7.91 (dd, J = 7.8, 2.1 Hz, 1H), 7.73 (m, 2H), 7.57 (td, J = 9.3, 2.4 Hz, 1H). FAB-MS m/z: 289 $[M + 1]^+$. Anal. ($C_{15}H_7ClF_2N_2$) C, H, N.

General Method[39] for the Preparation of the 11-Iodo-5-*N*-methyl-quindolinium Iodide Derivatives (4). A suspension of **3** (3 mmol), iodomethane (8 g), and sulfolane (15 g) was heated in a sealed flask overnight at 55 °C. A yellow precipitate was formed. The reaction mixture was allowed to cool to room temperature and then placed in an ice bath, precipitated further with a mixture of ice cold anhydrous diethyl ether (50 mL) and methanol (1 mL), filtered, andd washed thoroughly with anhydrous ethyl acetate to afford **4** as a yellow solid.

11-Iodo-5-*N*-methyl-10*H*-indolo[3,2-*b*]quinolinium Iodide (4a). Prepared as above using **3a** as starting materials. Yield 91%; mp 263−266 °C. ^{1}H NMR (DMSO-d_6, 300 Hz): δ 8.67 (d, J = 6.0 Hz, 1H), 8.56 (d, J = 9.0 Hz, 1H), 8.34 (d, J = 6.0 Hz, 1H), 8.01 (t, J = 6.0 Hz, 1H), 7.83 (d, J = 9.0 Hz, 1H), 7.72 (m, 2H), 7.37 (t, J = 6.0 Hz, 1H), 4.61 (s, 3H). ESI-MS m/z 359 $[M - I]^+$. Anal. ($C_{16}H_{12}I_2N_2 \cdot 1.3H_2O$) C, H, N.

11-Iodo-5-*N*-methyl-benzofuro[3,2-*b*]quinolinium Iodide (4b). Prepared as above using **3b** as starting materials. Yield 93%; mp 227−230 °C. ^{1}H NMR (DMSO-d_6, 300 Hz): δ 8.85 (d, J = 6.0 Hz, 1H), 8.77 (d, J = 9.0 Hz, 1H), 8.57 (d, J = 9.0 Hz, 1H), 8.31 (t, J = 6.0 Hz, 1H), 8.91 (d, J = 6.0 Hz, 1H), 8.13 (q, J = 9.0, 6.0 Hz, 2H), 7.79 (t, J = 6.0 Hz, 1H), 4.91 (s, 3H). ESI-MS m/z 360 $[M - I]^+$. Anal. ($C_{16}H_{11}I_2NO \cdot 0.5H_2O$) C, H, N.

7-Fluoro-11-iodo-5-*N*-methyl-10*H*-indolo[3,2-*b*]quinolinium Iodide (4c). Prepared as above using **3c** as starting materials. Yield 88%; mp 255−257 °C. ^{1}H NMR (DMSO-d_6, 300 Hz): δ 12.76 (s, 1H), 8.78 (d, J = 9.0 Hz, 1H), 8.69 (d, J = 9.0 Hz, 1H), 8.55 (d, J = 8.1 Hz, 1H), 8.20 (t, J = 7.5 Hz, 1H), 8.02 (t, J = 7.8 Hz, 1H), 7.89 (m, 2H), 4.93 (s, 3H). FAB-MS m/z 377 $[M - I]^+$. Anal. ($C_{16}H_{11}FI_2N_2$) C, H, N.

7,9-Difluoro-11-iodo-5-*N*-methyl-10*H*-indolo[3,2-*b*]quinolinium Iodide (4d). Prepared as above using **3d** as starting materials. Yield 90%; mp 235−238 °C. ^{1}H NMR (DMSO-d_6, 300 Hz): δ 8.87 (d, J = 9.0 Hz, 1H), 8.77 (t, J = 9.0 Hz, 1H), 8.53 (d, J = 9.0 Hz, 1H), 8.00 (m, 1H), 7.96 (d, J = 9.0 Hz, 1H), 7.86 (d, J = 9.0 Hz, 1H), 4.94 (s, 3H). FAB-MS m/z 395 $[M - I]^+$. Anal. ($C_{16}H_{10}F_2I_2N_2 \cdot 1.6H_2O$) C, H, N.

General Method for the Preparation of the 11-Alkylamido-5-*N*-methyl-quindolinium Iodide Derivatives (2). A suspension of **4** (0.4 mmol), *N*,*N*-dialkylalkylamine (10 mmol), and 2-ethoxyethanol (8 mL) was heated at 120 °C for 30 min. The reaction solution was allowed to cool to room temperature, added with ice-cold anhydrous diethyl ether (20 mL), and then placed at 4 °C overnight. A yellow precipitate was formed, which was filtered and washed thoroughly with anhydrous ethyl acetate to afford **2** as a yellow solid. Further purification was carried out by recrystallization from methanol−-diethyl ether (1:3).

***N*′-(5-*N*-Methyl-10*H*-indolo[3,2-*b*]quinolin-5-ium)-*N*,*N*-dimethyl-ethane-1,2-diamine iodide (2a).** Yield 80%; mp 208−209 °C. ^{1}H NMR (CDCl3, 300 Hz): δ 9.26 (d, J = 9.0 Hz, 1H), 8.29 (d, J = 9.0 Hz, 1H), 7.90 (t, J = 6.0 Hz, 2H), 7.67 (m, 3H), 7.33 (t, J = 9.0 Hz, 1H), 4.60 (s, 3H), 4.43 (m, 2H), 3.24 (d, J = 6 Hz, 2H), 2.58 (s, 6H). ^{13}C NMR (DMSO-d_6, 100 Hz): δ 143.0, 141.5, 136.9, 135.6, 132.1, 130.5, 124.2, 123.9, 123.7, 120.6, 117.3, 116.8, 115.1, 114.6, 113.5, 57.4, 43.8, 41.8, 38.0. FAB-MS m/z 319 $[M - I]^+$. FAB-HRMS m/z: calcd for $C_{20}H_{23}N_4$ $[M - I]^+$ 319.1917, found 319.1917. Anal. ($C_{20}H_{23}IN_4 \cdot 2.7H_2O$) C, H, N.

***N*′-(5-*N*-Methyl-10*H*-indolo[3,2-*b*]quinolin-5-ium)-*N*,*N*-dimethyl-propane-1,3-diamine Iodide (2b).** Yield 84%; mp 207−209 °C. ^{1}H NMR (DMSO-d_6, 300 Hz): δ 8.73 (d, J = 8.4 Hz, 1H), 8.54 (d, J = 8.4 Hz, 1H), 8.34 (d, J = 8.7 Hz, 1 H), 8.01 (t, J = 7.2 Hz, 2H), 7.91 (d, J = 8.7 Hz, 1H), 7.71 (m, 2H), 7.37 (t, J = 7.5 Hz, 1H), 4.60 (s, 3H), 4.23 (t, J = 6.3 Hz, 2H), 3.22 (t, J = 6.4 Hz, 2H), 2.76 (s, 6H), 2.22 (t, J = 7.2 Hz, 2H). ^{13}C NMR (DMSO-d_6, 100 Hz): δ 143.4, 142.6, 137.0, 135.4, 132.2, 130.4, 124.1, 124.1, 123.8, 120.6, 117.2, 116.2, 115.0, 114.3, 113.5, 54.1, 42.7, 42.2, 42.2, 37.9, 24.6. FAB-MS m/z 333 $[M - I]^+$. FAB-HRMS m/z: calcd for $C_{21}H_{25}N_4$ $[M - I]^+$ 333.2079, found 333.2070. Anal. ($C_{21}H_{25}IN_4 \cdot 1.9H_2O$) C, H, N.

***N′*-(5-*N*-Methyl-10*H*-indolo[3,2-*b*]quinolin-5-ium)-*N*,*N*-diethyl-ethane-1,2-diamine Iodide (2c).** Yield 78%; mp 180−182 °C. ^{1}H NMR (CDCl3, 300 Hz): δ 9.31 (d, *J* = 8.7 Hz, 1H), 8.29(d, *J* = 8.4 Hz, 1H), 7.88 (t, *J* = 7.2 Hz, 2 H), 7.66 (m, 3H), 7.33 (t, *J* = 7.4 Hz, 1H), 4.60 (s, 3 H), 4.39 (brs, 2H), 3.28 (brs, 2H), 2.85 (m, 4H), 1.13 (t, *J* = 6.3 Hz, 6H). ^{13}C NMR (DMSO-d_6, 100 Hz): δ 143.2, 142.8, 136.7, 135.6, 132.0, 130.3, 124.1, 123.8, 123.7, 122.9, 120.4, 117.1, 115.0, 114.4, 113.3, 54.8, 46.5, 46.5, 41.9, 37.8, 10.7, 10.7. FAB-MS *m*/*z* 347 [M − I]$^+$. FAB-HRMS *m*/*z*: calcd for $C_{22}H_{27}N_4$ [M − I]$^+$ 347.2230, found 347.2287. Anal. ($C_{22}H_{27}IN_4 \cdot 2.1H_2O$) C, H, N.

***N′*-(5-*N*-Methyl-10*H*-indolo[3,2-*b*]quinolin-5-ium)-*N*,*N*-diethyl-propane-1,3-diamine Iodide (2d).** Yield 87%; mp 206−208 °C. ^{1}H NMR (DMSO-d_6, 300 Hz): δ 8.54 (m, 2H), 8.31 (t, *J* = 9.0 Hz, 1H), 7.99 (dd, *J* = 9.0, 2.0 Hz, 1 H), 7.67 (m, 3H), 7.35 (t, *J* = 9.0 Hz, 1H), 4.53 (s, 3H), 4.32 (t, *J* = 6.0 Hz, 2H), 2.87 (q, *J* = 3.0 Hz, 2H), 2.74 (brs, 2H), 2.07 (m, 2H), 0.97 (s, 6H). ^{13}C NMR (DMSO-d_6, 100 Hz): δ 144.7, 143.9, 136.7, 134.3, 131.8, 130.2, 124.1, 123.4, 122.6, 120.3, 117.2, 116.4, 115.4, 114.4, 113.5, 47.9, 45.8, 45.8, 43.5, 37.5, 25.5, 9.6, 9.6. FAB-MS *m*/*z* 361 [M − I]$^+$. FAB-HRMS *m*/*z*: calcd for $C_{23}H_{29}N_4$ [M − I]$^+$ 361.2387, found 361.2415. Anal. ($C_{23}H_{29}IN_4 \cdot 1.7H_2O$) C, H, N.

***N′*-(5-*N*-Methyl-10*H*-indolo[3,2-*b*]quinolin-5-ium)-(2-morpholin-4-yl-ethyl)-amine Iodide (2e).** Yield 90%; mp 240−242 °C. ^{1}H NMR (DMSO-d_6, 300 Hz): δ 8.59 (dd, *J* = 8.4, 3.3 Hz, 2H), 8.35 (d, *J* = 8.7 Hz, 1H), 8.02 (t, *J* = 8.4 Hz, 1H), 7.87 (t, *J* = 7.2 Hz, 1H), 7.74 (dd, *J* = 7.8, 6.9 Hz, 2H), 7.39 (t, *J* = 7.8 Hz, 1H), 4.62 (s, 3H), 4.21 (t, *J* = 5.7 Hz, 2H), 3.51 (t, *J* = 4.5 Hz, 4H), 2.83 (t, *J* = 5.7 Hz, 2H), 2.53 (s, 4H). ^{13}C NMR (DMSO-d_6, 100 Hz): δ 143.7, 142.4, 137.0, 135.4, 132.2, 130.5, 124.3, 124.0, 123.5, 120.7, 117.3, 116.7, 115.1, 114.7, 113.4, 65.9, 65.9, 57.3, 53.3, 53.3, 42.9, 37.9. FAB-MS *m*/*z* 361 [M − I]$^+$. FAB-HRMS *m*/*z*: calcd for $C_{22}H_{25}N_4O$ [M − I]$^+$ 361.2023, found 361.2047. Anal. ($C_{22}H_{25}IN_4O \cdot 1.1H_2O$) C, H, N.

***N′*-(5-*N*-Methyl-10*H*-indolo[3,2-*b*]quinolin-5-ium)-(3-morpholin-4-yl-propyl)-amine Iodide (2f).** Yield 90%; mp 220−223 °C. ^{1}H NMR ($CDCl_3$, 300 Hz): δ 9.33 (m, 1H), 8.67 (d, *J* = 9.0 Hz, 1H), 8.17 (dd, *J* = 6.0, 3.0 Hz, 2H), 7.96 (m, 2H), 7.60 (t, *J* = 9.0 Hz, 1H), 7.50 (t, *J* = 9.0 Hz, 1H), 4.55 (s, 3H), 3.82 (t, *J* = 6.0 Hz, 4H), 2.74 (t, *J* = 3.0 Hz, 2H), 2.61 (t, *J* = 3.0 Hz, 4H), 2.29 (m, 2H). ^{13}C NMR (DMSO-d_6, 100 Hz): δ 143.8, 142.4, 137.1, 135.5, 132.2, 130.4, 124.2, 123.9, 123.7, 117.3, 116.2, 115.1, 114.5, 113.4, 65.8, 65.8, 55.5, 53.1, 53.1, 43.9, 37.9, 25.6. FAB-MS *m*/*z* 375 [M − I]$^+$. FAB-HRMS *m*/*z*: calcd for $C_{23}H_{27}N_4O$ [M − I]$^+$ 375.2185, found 375.2234. Anal. ($C_{23}H_{27}IN_4O \cdot 0.9H_2O$) C, H, N.

***N′*-(5-*N*-Methyl-10*H*-indolo[3,2-*b*]quinolin-5-ium)-2-aminoethanol Iodide (2g).** Yield 92%; mp 235−237 °C. ^{1}H NMR (DMSO-d_6, 300 Hz): δ 8.67 (d, *J* = 6.0 Hz, 1H), 8.56 (d, *J* = 9.0 Hz, 1H), 8.34 (d, *J* = 9.0 Hz, 1H), 8.02 (t, *J* = 6.0 Hz, 1H), 7.83 (d, *J* = 9.0 Hz, 1H), 7.73 (m, 2H), 7.38 (t, *J* = 9.0 Hz, 1H), 4.62 (s, 3H), 4.17 (m, 2H), 3.85 (m, 2H). ^{13}C NMR (DMSO-d_6, 100 Hz): δ 144.1, 142.2, 137.0, 135.3, 132.1, 130.4, 124.1, 123.8, 123.7, 120.6, 117.2, 116.3, 115.1, 114.5, 113.4, 60.1, 47.7, 37.8. FAB-MS *m*/*z* 292 [M − I]$^+$. FAB-HRMS *m*/*z*: calcd for $C_{18}H_{18}N_3O$ [M − I]$^+$ 292.1444, found 292.1470. Anal. ($C_{18}H_{18}IN_3O \cdot H_2O$) C, H, N.

***N′*-(5-*N*-Methyl-10*H*-indolo[3,2-*b*]quinolin-5-ium)-3-aminopropanol Iodide (2h).** Yield 88%; mp 203−207 °C. ^{1}H NMR (DMSO-d_6, 300 Hz): δ 8.63 (d, *J* = 9.4 Hz, 1H), 8.55 (d, *J* = 8.4 Hz, 1H), 8.34 (d, *J* = 9.3 Hz, 1H), 8.01 (t, *J* = 7.5 Hz, 1H), 7.74 (m, 3H), 7.39 (t, *J* = 6.9 Hz, 1H), 4.61 (s, 3H), 4.18 (m, 2H), 3.64 (m, 2H), 2.02 (m, 2H). ^{13}C NMR (DMSO-d_6, 100 Hz): δ 143.7, 142.4, 137.1, 135.2, 132.1, 130.3, 124.1, 123.8, 123.7, 120.5, 117.2, 116.2, 115.0, 114.3, 113.3, 57.8, 42.4, 37.8, 32.3. FAB-MS *m*/*z* 306 [M − I]$^+$. FAB-HRMS *m*/*z*: calcd for $C_{19}H_{20}N_3O$ [M − I]$^+$ 306.1601, found 306.1590. Anal. ($C_{19}H_{20}IN_3O \cdot 2.5H_2O$) C, H, N.

***N′*-(5-*N*-Methyl-benzofuro[3,2-*b*]quinolin-5-ium)-*N*,*N*-dimethyl-ethane-1,2-diamine Iodide (2i).** Yield 85%; mp 162−163 °C. ^{1}H NMR (DMSO-d_6, 300 Hz): δ 8.62 (d, *J* = 9.0 Hz, 2H), 8.32 (d, *J* = 8.7 Hz, 1H), 8.07 (t, *J* = 7.5 Hz, 1H), 7.78 (m, 1H), 7.65 (t, *J* = 6.9 Hz, 1H), 4.54 (s, 3H), 4.20 (m, 2H), 2.74 (m, 2H), 2.21 (s, 6H). FAB-MS *m*/*z* 320 [M − I]$^+$. ^{13}C NMR (DMSO-d_6, 100 Hz): δ 156.6, 142.2, 138.4, 138.0, 133.2, 132.7, 131.4, 125.3, 124.9, 124.5, 123.9, 117.9, 116.8, 116.5, 113.0, 58.8, 45.2, 45.2, 43.3, 37.5 FAB-HRMS *m*/*z*: calcd for $C_{20}H_{22}N_3O$ [M − I]$^+$ 320.1757, found 320.1773. Anal. ($C_{20}H_{22}IN_3O \cdot 3.2H_2O$) C, H, N.

***N′*-(5-*N*-Methyl-benzofuro[3,2-*b*]quinolin-5-ium)-*N*,*N*-dimethyl-propane-1,2-diamine Iodide (2j).** Yield 83%; mp 190−192 °C. ^{1}H NMR ($CDCl_3$, 300 Hz): δ 8.58 (d, *J* = 8.7 Hz, 1H), 8.44 (d, *J* = 7.8 Hz, 1H), 8.18 (t, *J* = 8.7 Hz, 1H), 7.78 (m, 2H), 7.60 (m, 2H), 4.65 (s, 3H), 4.40 (m, 2H), 2.74 (m, 2H), 2.42 (s, 6H), 2.13 (m, 2H). ^{13}C NMR (DMSO-d_6, 100 Hz): δ 156.6, 142.1, 138.2, 137.9, 133.1, 132.6, 131.4, 125.3, 124.8, 124.5, 123.7, 117.8, 116.7, 116.4, 113.0, 56.6, 44.8, 44.8, 44.5, 37.4, 27.3. FAB-MS *m*/*z* 334 [M − I]$^+$. FAB-HRMS *m*/*z*: calcd for $C_{21}H_{24}N_3O$ [M − I]$^+$ 334.1914, found 334.1939. Anal. ($C_{21}H_{24}IN_3O \cdot 1.8H_2O$) C, H, N.

***N′*-(5-*N*-Methyl-benzofuro[3,2-*b*]quinolin-5-ium)-*N*,*N*-diethyl-ethane-1,2-diamine Iodide (2k).** Yield 84%; mp 179−180 °C. ^{1}H NMR (DMSO-d_6, 300 Hz): δ 8.60 (d, *J* = 8.7 Hz, 1H), 8.35 (d, *J* = 9.0 Hz, 1H), 8.08 (t, *J* = 7.2 Hz, 1H), 7.93 (m, 2H), 7.78 (t, *J* = 7.8 Hz, 1H), 7.67 (m, 2H), 4.54 (s, 3H), 4.20 (t, *J* = 6.6 Hz, 2H), 2.85 (t, *J* = 6.9 Hz, 2H), 2.60 (q, *J* = 6.9 Hz, 4H), 0.92 (t, *J* = 6.9 Hz, 6H). ^{13}C NMR (DMSO-d_6, 100 Hz): δ 156.2, 142.1, 138.1, 137.7, 132.9, 132.5, 131.2, 131.2, 125.1, 124.7, 124.3, 123.6, 117.7, 116.5, 116.2, 112.7, 52.3, 46.6, 46.6, 43.5, 37.3, 11.7,11.7. FAB-MS *m*/*z* 348 [M − I]$^+$. FAB-HRMS *m*/*z*: calcd for $C_{22}H_{26}N_3O$ [M − I]$^+$ 348.2070, found 348.2052. Anal. ($C_{22}H_{26}IN_3O \cdot 2.2H_2O$) C, H, N.

***N′*-(5-*N*-Methyl-benzofuro[3,2-*b*]quinolin-5-ium)-*N*,*N*-diethyl-propane-1,2-diamine Iodide (2l).** Yield 80%; mp 168−170 °C. ^{1}H NMR ($CDCl_3$, 300 Hz): δ 8.58 (d, *J* = 8.4 Hz, 1H), 8.46 (d, *J* = 8.1 Hz, 1H), 8.22 (t, *J* = 9.0 Hz, 1H), 7.96 (t, *J* = 7.2 Hz, 2H), 7.75 (m, 2H), 7.60 (m, 2H), 4.67 (s, 3H), 4.40 (t, *J* = 6.3 Hz, 2H), 2.86 (t, *J* = 6.9 Hz, 2H), 2.76 (q, *J* = 7.2 Hz, 4H), 2.12 (m, 2H), 1.12 (t, *J* = 7.2 Hz, 6H). ^{13}C NMR (DMSO-d_6, 100 Hz): δ 156.5, 142.1, 138.2, 137.9, 133.1, 132.6, 131.5, 125.1, 124.8, 124.5, 123.8, 117.8, 116.8, 116.5, 112.9, 49.9, 46.1, 46.1, 44.8, 37.4, 27.0, 11.3, 11.3. FAB-MS *m*/*z* 362 [M − I]$^+$. FAB-HRMS *m*/*z*: calcd for $C_{23}H_{28}N_3O$ [M − I]$^+$ 362.2227, found 362.2252. Anal. ($C_{23}H_{28}IN_3O \cdot 1.6H_2O$) C, H, N.

***N′*-(5-*N*-Methyl-benzofuro[3,2-*b*]quinolin-5-ium)-(2-morpholin-4-yl-ethyl)-amine Iodide (2m).** Yield 89%; mp 186−187 °C. ^{1}H NMR (DMSO-d_6, 300 Hz): δ 8.61 (d, *J* = 9.0 Hz, 1H), 8.35 (d, *J* = 9.0 Hz, 1H), 8.07 (t, *J* = 9.0 Hz, 1H), 7.94 (m, 2H), 7.77 (t, *J* = 9.0 Hz, 1H), 7.65 (t, *J* = 9.0 Hz, 1H), 4.52 (s, 3H), 4.19 (t, *J* = 6.0 Hz, 2H), 3.65 (m, 4H), 3.65 (t, *J* = 6.0 Hz, 4H), 2.77 (t, *J* = 6.0 Hz, 2H). ^{13}C NMR (DMSO-d_6, 100 Hz): δ 156.6, 142.2, 138.5, 137.9, 133.2, 132.8, 131.4, 125.4, 124.9, 124.6, 123.8, 118.0, 116.7, 116.3, 113.0, 66.1, 66.1, 58.0, 53.2, 53.2, 42.5, 37.6. FAB-MS *m*/*z* 362 [M − I]$^+$. FAB-HRMS *m*/*z*: calcd for $C_{22}H_{24}N_3O_2$ [M − I]$^+$ 362.1863, found 362.1858. Anal. ($C_{22}H_{24}IN_3O_2 \cdot 1.3H_2O$) C, H, N.

***N′*-(5-*N*-Methyl-benzofuro[3,2-*b*]quinolin-5-ium)-(3-morpholin-4-yl-propyl)-amine Iodide (2n).** Yield 87%; mp 193−195 °C. ^{1}H NMR ($CDCl_3$, 300 Hz): δ 9.21 (d, *J* = 9.0 Hz, 1H), 8.40 (d, *J* = 9.0 Hz, 1H), 8.03 (d, *J* = 9.0 Hz, 1H), 7.89 (t, *J* = 9.0 Hz, 1H), 7.81 (t, *J* = 6.0 Hz, 1H), 7.73 (d, *J* = 6.0 Hz, 1H), 7.60 (m, 2H), 4.61 (s, 3H), 4.36 (t, *J* = 9.0 Hz, 2H), 3.69 (t, *J* = 3.0 Hz, 2H), 2.69 (t, *J* = 6.0 Hz, 2H), 2.55 (t, *J* = 3.0 Hz, 4H), 2.17 (m, 2H). ^{13}C NMR (DMSO-d_6, 100 Hz): δ 157.2, 142.8, 139.1, 138.5, 133.8, 133.4, 131.9, 125.9, 125.5, 125.2, 124.6, 118.5, 117.3, 117.0, 113.6, 66.6, 66.6, 56.3, 53.8, 53.8, 44.7, 38.2, 27.3. FAB-MS *m*/*z* 376 [M − I]$^+$. FAB-HRMS *m*/*z*: calcd for $C_{23}H_{26}N_3O_2$ [M − I]$^+$ 376.2020, found 376.2029. Anal. ($C_{23}H_{26}IN_3O_2 \cdot 0.8H_2O$) C, H, N.

***N′*-(5-*N*-Methyl-benzofuro[3,2-*b*]quinolin-5-ium)-2-aminoethanol Iodide (2o).** Yield 92%; mp 145−146 °C. ^{1}H NMR (DMSO-d_6, 300 Hz): δ 8.67 (d, *J* = 9.0 Hz, 1H), 8.59 (d, *J* = 9.0 Hz, 1H), 8.31 (d, *J* = 9.0 Hz, 1H), 8.05 (t, *J* = 9.0 Hz, 1H), 7.91 (m, 2H), 7.72 (t, *J* = 9.0 Hz 1H), 7.63 (t, *J* = 9.0 Hz, 1H), 4.51 (s, 3H), 4.19 (t, *J* = 6.0 Hz, 2H), 3.82 (t, *J* = 6.0 Hz, 2H). ^{13}C NMR (DMSO-d_6, 100 Hz): δ 156.3, 142.3, 138.2, 137.6, 133.0, 132.5,

131.2, 125.0, 124.6, 124.3, 123.9, 117.6, 116.4, 116.2, 112.9, 60.1, 47.7, 37.3. FAB-MS *m/z* 293 $[M - I]^+$. FAB-HRMS *m/z*: calcd for $C_{18}H_{17}N_2O_2$ $[M - I]^+$ 293.1285, found 293.1286. Anal. ($C_{18}H_{17}IN_2O_2 \cdot 0.4H_2O$) C, H, N.

***N′*-(5-*N*-Methyl-benzofuro[3,2-*b*]quinolin-5-ium)-3-amino-propanol Iodide (2p).** Yield 91%; mp 170−172 °C. ^{1}H NMR (DMSO-d_6, 300 Hz): δ 8.60 (t, $J = 7.5$ Hz, 2H), 8.34 (d, $J = 8.7$ Hz, 1H), 8.06 (t, $J = 7.5$ Hz, 1H), 7.92 (m, 2H), 7.76 (t, $J = 7.5$ Hz, 1H), 7.64 (t, $J = 7.2$ Hz, 1H), 4.51 (s, 3H), 4.16 (t, $J = 6.9$ Hz, 2H), 3.63 (t, $J = 6.0$ Hz, 6H), 1.99 (m, 2H). FAB-MS *m/z* 307 $[M - I]^+$. ^{13}C NMR (DMSO-d_6, 100 Hz): δ 156.6, 142.1, 138.4, 137.8, 133.1, 132.6, 131.2, 125.2, 124.8, 124.5, 123.9, 117.8, 116.6, 116.3, 113.1, 58.2, 43.0, 37.5, 33.2. FAB-HRMS *m/z*: calcd for $C_{19}H_{19}N_2O_2$ $[M - I]^+$ 307.1441, found 307.1446. Anal. ($C_{19}H_{19}IN_2O_2 \cdot 1.9H_2O$) C, H, N.

***N′*-(7-Fluoro-5-*N*-methyl-10*H*-indolo[3,2-*b*]quinolin-5-ium)-*N*,*N*-dimethyl-ethane-1,2-diamine Iodide (2q).** Yield 83%; mp 245−247 °C. ^{1}H NMR (DMSO-d_6, 300 Hz): δ 8.61 (d, $J = 8.4$ Hz, 1H), 8.37 (m, 2H), 8.01 (t, $J = 8.1$ Hz, 1 H), 7.84 (q, $J = 4.8$ Hz, 1H), 7. 67 (m, 2H), 4.57 (s, 3H), 4.19 (t, $J = 5.1$ Hz, 2H), 2.95 (m, 2H), 2.44 (s, 6H). ^{13}C NMR (DMSO-d_6, 100 Hz): δ 157.6, 155.3, 144.2, 139.9, 137.0, 134.7, 132.2, 123.7, 123.5, 118.7, 117.2, 115.3, 114.7, 108.9, 108.6, 58.5, 44.6, 44.6, 43.2, 37.6. FAB-MS *m/z* 337 $[M - I]^+$. FAB-HRMS *m/z*: calcd for $C_{20}H_{22}FN_4$ $[M - I]^+$ 337.1823, found 337.1768. Anal. ($C_{20}H_{22}FIN_4 \cdot 1.2H_2O$) C, H, N.

***N′*-(7-Fluoro-5-*N*-methyl-10*H*-indolo[3,2-*b*]quinolin-5-ium)-*N*,*N*-dimethyl-propane-1,3-diamine Iodide (2r).** Yield 84%; mp 230−232 °C. ^{1}H NMR ($CDCl_3$, 300 Hz): δ 9.74 (brs, 1H), 9.07 (d, $J = 8.7$ Hz, 1H), 7.88 (m, 3H), 7.73 (q, $J = 4.5$ Hz, 1H), 7.61 (t, $J = 7.8$ Hz, 1H), 7.32 (td, $J = 8.7$, 2.1 Hz, 1H), 4.52 (s, 3H), 4.46 (t, $J = 5.1$ Hz, 2H), 2.72 (t, $J = 5.7$ Hz, 2H), 2.43 (s, 6H), 2.37 (m, 2H). ^{13}C NMR (DMSO-d_6, 100 Hz): δ 157.5, 155.1, 144.9, 140.5, 136.9, 135.2, 132.1, 123.4, 119.1, 117.1, 115.5, 114.7, 114.4, 108.7, 108.5, 54.1, 43.3, 43.3, 42.9, 37.5, 25.8. FAB-MS *m/z* 351 $[M - I]^+$. FAB-HRMS *m/z*: calcd for $C_{21}H_{24}FN_4$ $[M - I]^+$ 351.1980, found 351.1953. Anal. ($C_{21}H_{24}FIN_4 \cdot 3.2H_2O$) C, H, N.

***N′*-(7-Fluoro-5-*N*-methyl-10*H*-indolo[3,2-*b*]quinolin-5-ium)-*N*,*N*-diethyl-ethane-1,2-diamine Iodide (2s).** Yield 80%; mp 232−234 °C. ^{1}H NMR (CDCl3, 300 Hz): δ 8.58 (d, $J = 7.8$ Hz, 1H), 8.41 (d, $J = 9.0$ Hz, 1H), 8.35 (d, $J = 9.0$ Hz, 1H), 8.00 (t, $J = 7.5$ Hz, 1H), 7.77 (q, $J = 4.5$ Hz, 1H), 7.69 (t, $J = 7.5$ Hz, 1H), 7.62 (td, $J = 9.0$, 2.4 Hz, 1H), 4.57 (s, 3 H), 4.14 (t, $J = 5.4$ Hz, 2H), 3.00 (t, $J = 5.4$ Hz, 2H), 2.85 (q, $J = 6.9$ Hz, 4H), 0.96 (t, $J = 6.9$ Hz, 6H). ^{13}C NMR (DMSO-d_6, 100 Hz): δ 158.2, 155.8, 145.0, 140.6, 137.6, 135.4, 132.8, 124.3, 123.9, 119.8, 117.9, 115.8, 115.3, 109.6, 109.3, 53.4, 47.7, 47.7, 44.7, 38.1, 11.1, 11.1. FAB-MS *m/z* 365 $[M - I]^+$. FAB-HRMS *m/z*: calcd for $C_{22}H_{26}FN_4$ $[M - I]^+$ 365.2136, found 365.2193. Anal. ($C_{22}H_{26}FIN_4 \cdot 2.4H_2O$) C, H, N.

***N′*-(7-Fluoro-5-*N*-methyl-10*H*-indolo[3,2-*b*]quinolin-5-ium)-*N*,*N*-diethyl-propane-1,3-diamine Iodide (2t).** Yield 82%; mp 216−218 °C. ^{1}H NMR (DMSO-d_6, 300 Hz): δ 8.54 (d, $J = 8.9$ Hz, 1H), 8.32 (t, $J = 9.0$ Hz, 1H), 7.98 (t, $J = 9.0$ Hz, 1 H), 7.77 (q, $J = 6.0$ Hz, 1H), 7.57 (td, $J = 9.0$, 3.0 Hz, 1H), 4.54 (s, 3H), 4.26 (t, $J = 6.0$ Hz, 2H), 2.77 (q, $J = 6.0$ Hz, 2H), 2.05 (m, 2H), 0.96 (t, $J = 6.0$ Hz, 6H). ^{13}C NMR (DMSO-d_6, 100 Hz): δ 158.0, 155.7, 145.1, 141.3, 137.5, 135.5, 132.6, 124.0, 124.0, 119.2, 117.7, 116.3, 115.1, 109.2, 109.0, 48.8, 46.5, 46.5, 44.4, 38.1, 26.2, 10.5, 10.5. FAB-MS *m/z* 379 $[M - I]^+$. FAB-HRMS *m/z*: calcd for $C_{23}H_{28}FN_4$ $[M - I]^+$ 379.2293, found 379.2319. Anal. ($C_{23}H_{28}FIN_4 \cdot 1.5H_2O$) C, H, N.

***N′*-(7,9-Difluoro-5-*N*-methyl-10*H*-indolo[3,2-*b*]quinolin-5-ium)-*N*,*N*-dimethyl-ethane-1,2-diamine Iodide (2u).** Yield 80%; mp 238−240 °C. ^{1}H NMR (DMSO-d_6, 300 Hz): δ 8.56 (d, $J = 9.0$ Hz, 1H), 8.29 (d, $J = 9.0$ Hz, 1H), 8.14 (d, $J = 9.0$ Hz, 1 H), 7.94 (t, $J = 9.0$ Hz, 1H), 7.62 (t, $J = 9.0$ Hz, 1H), 7.47 (t, $J = 9.0$ Hz, 1H), 4.53 (s, 3H), 4.44 (t, $J = 6.0$ Hz, 2H), 3.37 (t, $J = 6.0$ Hz, 2H), 2.75 (s, 6H). ^{13}C NMR (DMSO-d_6, 100 Hz): δ 155.7, 153.2, 146.1, 137.2, 135.2, 132.1, 130.2, 125.0, 124.0, 123.3, 117.4, 116.3, 114.5, 104.7, 103.4, 59.4, 44.3, 44.3, 42.6, 37.8. FAB-MS *m/z* 355 $[M - I]^+$. FAB-HRMS *m/z*: calcd for $C_{20}H_{21}F_2N_4$ $[M - I]^+$ 355.1729, found 355.1733. Anal. ($C_{20}H_{21}F_2IN_4 \cdot 1.4H_2O$) C, H, N.

***N′*-(7,9-Difluoro-5-*N*-methyl-10*H*-indolo[3,2-*b*]quinolin-5-ium)-*N*,*N*-dimethyl-propane-1,3-diamine Iodide (2v).** Yield 86%; mp 250−253 °C. ^{1}H NMR (DMSO-d_6, 300 Hz): δ 8.59 (d, $J = 8.4$ Hz 1H), 8.26 (d, $J = 9.0$ Hz, 1H), 8.11 (d, $J = 9.0$ Hz, 1H), 7.92 (t, $J = 7.5$ Hz, 1H), 7.59 (t, $J = 8.4$ Hz, 1H), 7.42 (t, $J = 9.0$ Hz, 1H), 4.51 (s, 3H), 4.51 (m, 2H), 3.14 (t, $J = 5.7$ Hz, 2H), 2.68 (s, 6H), 2.20 (m, 2H). ^{13}C NMR (DMSO-d_6, 100 Hz): δ 154.7, 152.5, 149.7, 146.6, 136.5, 135.1, 131.4, 125.6, 123.6, 122.3, 116.6, 115.9, 113.9, 103.6, 102.3, 62.7, 52.4, 41.5, 41.5, 37.0, 25.1. FAB-MS *m/z* 369 $[M - I]^+$. FAB-HRMS *m/z*: calcd for $C_{21}H_{23}F_2N_4$ $[M - I]^+$ 369.2185, found 369.2194. Anal. ($C_{21}H_{23}F_2IN_4 \cdot 2.3H_2O$) C, H, N.

***N′*-(7,9-Difluoro-5-*N*-methyl-10*H*-indolo[3,2-*b*]quinolin-5-ium)-*N*,*N*-diethyl-ethane-1,2-diamine Iodide (2w).** Yield 83%; mp 240−243 °C. ^{1}H NMR (CD_3OD, 300 Hz): δ 8.48 (d, $J = 8.4$ Hz, 1H), 8.23 (d, $J = 9.0$ Hz, 1H), 8.06 (d, $J = 9.0$ Hz, 1H), 7.97 (t, $J = 7.2$ Hz, 1H), 7.65 (t, $J = 7.5$ Hz, 1H), 7.35 (t, $J = 9.0$ Hz, 1H), 4.56 (s, 3 H), 4.32 (t, $J = 4.2$ Hz, 2H), 3.30 (m, 2H), 2.98 (q, $J = 7.2$ Hz, 4H), 1.10 (t, $J = 7.2$ Hz, 6H). ^{13}C NMR (DMSO-d_6, 100 Hz): δ 154.7, 152.4, 145.2, 136.3, 134.5, 131.3, 124.7, 123.2, 122.4, 116.6, 115.9, 115.8, 113.6, 103.9, 102.6, 52.9, 47.8, 47.8, 42.1, 37.0, 8.7, 8.7. FAB-MS *m/z* 383 $[M - I]^+$. FAB-HRMS *m/z*: calcd for $C_{22}H_{25}F_2N_4$ $[M - I]^+$ 383.2042, found 383.2049. Anal. ($C_{22}H_{25}F_2IN_4 \cdot 1.1H_2O$) C, H, N.

***N′*-(7,9-Difluoro-5-*N*-methyl-10*H*-indolo[3,2-*b*]quinolin-5-ium)-*N*,*N*-diethyl-propane-1,3-diamine Iodide (2x).** Yield 82%; mp 253−254 °C. ^{1}H NMR (DMSO-d_6, 300 Hz): δ 8.60 (d, $J = 8.7$ Hz, 1H), 8.26 (d, $J = 9.0$ Hz, 1H), 8.11 (m, 1 H), 7.93 (t, $J = 8.1$ Hz, 1H), 7.59 (t, $J = 7.5$ Hz, 1H), 7.42 (m, 1 H), 4.57 (m, 2H), 4.51 (s, 3H), 3.22 (t, $J = 6.6$ Hz, 2H), 3.14 (q, $J = 5.4$ Hz, 4H), 2.20 (m, 2H), 0.98 (t, $J = 5.4$ Hz, 6H). ^{13}C NMR (DMSO-d_6, 100 Hz): δ 157.2, 154.8, 144.3, 140.4, 136.7, 134.7, 131.8, 123.1, 119.0, 118.3, 116.9, 115.4, 114.3, 108.4, 108.1, 48.0, 45.6, 45.6, 43.6, 37.2, 25.4, 9.7, 9.7. FAB-MS *m/z* 397 $[M - I]^+$. FAB-HRMS *m/z*: calcd for $C_{23}H_{27}F_2N_4$ $[M - I]^+$ 397.2198, found 397.2221. Anal. ($C_{23}H_{27}F_2IN_4 \cdot 0.9H_2O$) C, H, N.

Materials. All oligomers/primers used in this study were purchased from Invitrogen (China). Acrylamide/ bisacrylamide solution and *N,N,N′,N′*-tetramethyl-ethylenediamine were purchased from Sigma. *Taq* DNA polymerase was purchased from Sangon, China. Stock solutions of all the derivatives (10 mM) were made using DMSO (10%) or double-distilled deionized water. Further dilutions to working concentrations were made with double-distilled deionized water. All tumor cell lines were obtained from the American Type Culture Collection (ATCC, Rockville, MD). The cell culture was maintained in a RPMI-1640 medium supplemented with 10% fetal bovine serum, 100 U/mL penicillin, and 100 μg/mL streptomycin in 25 cm^2 culture flasks at 37 °C humidified atmosphere with 5% CO_2.

CD Measurements. CD measurements were performed on a Chirascan circular dichroism spectrophotometer (Applied Photophysics) using a quartz cuvettes of 2 mm optical path length and over a wavelength range of 230−450 at 1 nm bandwidth, 1 nm step size, and 0.5 s time per point. The oligomer HTG21 d[GGG(TTAGGG)$_3$] at a final concentration of 5 μM was resuspended in Tris-HCl buffer (10 mM, pH 7.4) containing the specific cations and the compounds to be tested. The samples were heated to 95 °C for 5 min, then gradually cooled to room temperature and incubated at 4 °C overnight. A buffer baseline was collected in the same cuvette and subtracted from the sample spectra. The CD spectra were obtained by taking the average of at least three scans at 25 °C. Then, CD titration was performed at a fixed HTG21 concentration (5 μM) with various concentrations (0−5 mol equiv) of the compounds in Tris-HCl buffer with 100 mM KCl. After each addition of compound, the reaction was stirred and allowed to equilibrate for at least 15 min (until no elliptic changes were observed) and a CD spectrum was collected. Final analysis of the data was carried out using Origin 7.5 (OriginLab Corp.).

Table 4. Nucleic Acid Conformation and Samples Used in Competition Dialysis Experiments

conformation	DNA/oligonucleotide	$\varepsilon/M^{-1}\cdot\chi\mu^{-1}$	description
single strand DNA	dA21	255400	multiple mutant oligomer of HTG21 that may not form G-quadruplex
	dT21	170700	
	HTG21mu:d[GAG(TTAGAG)$_3$]	257400	
duplex DNA	dA21:dT21	12000	human telomere/complementary
	HTds:d[G$_3$(T$_2$AG$_3$)$_3$]/d[C$_3$(TA$_2$C$_3$)$_3$]	11403	
triplex DNA	dA21: (dT21)$_2$	17200	
quadruplex DNA	HTG21:d[G$_3$(T$_2$AG$_3$)$_3$]	73000	partial sequence in human telomere may form intramolecular G-quadruplex
	Pu27:d(TG$_4$AG$_3$TG$_4$AG$_3$TG$_4$A$_2$G$_2$)	45309	partial sequence oncogene *c-myc* that may form G-quadruplex
	HT-7:d(T$_2$AG$_3$T)	19500	partial sequence of HTG21 that may form intermolecular G-quadruplex
i-motif	HTC21:d[C$_3$(TA$_2$C$_3$)$_3$]	148720	complementary sequence of HTG21 that may form an i-motif structure

FRET Assay. FRET assay was carried out on a real-time PCR apparatus (Roche LightCycler 2) following previously published procedures.[45] The fluorescent labeled oligonucleotide F21T [5′-FAM- d(GGG[TTAGGG]$_3$)-TAMRA-3′], donor fluorophore *FAM*, 6-carboxyfluorescein, acceptor fluorophore *TAMRA*, and 6-carboxytetramethylrhodamine] used as the FRET probes were diluted from stock to the correct concentration (400 nM) in Tris-HCl buffer (10 mM, pH 7.4) containing 60 mM KCl and then annealed by heating to 90 °C for 5 min, followed by cooling to room temperature. Samples were prepared by aliquoting 10 μL of the annealed F21T (at 2× concentration, 400 nM) into LightCycler capillaries, followed by 10 μL of the compound solutions (at 2× concentration, 2 μM) and further incubated for 1 h. Measurements were made in triplicate on a RT-PCR with excitation at 470 nm and detection at 530 nm. Fluorescence readings were taken at intervals of 1 °C over the range 37−99 °C, with a constant temperature being maintained for 30 s prior to each reading to ensure a stable value. Final analysis of the data was carried out using Origin 7.5 (OriginLab Corp.).

PCR Stop Assay. The PCR stop assay was conducted according to a modified protocol of the previous study.[47] The oligonucleotide HTG21 d[GGG(TTAGGG)$_3$] and the corresponding complementary sequence d(ATCGCT$_2$CTCGTC$_3$TA$_2$C$_2$) were used here. The reaction were performed in 1× PCR buffer, containing with 10 pmol of each oligonucleotide, 0.16 mM dNTP, 2.5 U *Taq* polymerase, and the compounds to be tested. Reaction mixtures were incubated in a thermocycler with the following cycling conditions: 94 °C for 3 min, followed by 30 cycles of 94 °C for 30 s, 58 °C for 30 s, and 72 °C for 30 s. Amplified products were resolved on 15% nondenaturing polyacrylamide gels in 1× TBE and silver stained. IC_{50} values were calculated using optical density read from LadWorks software.

NMR Spectroscopy. NMR experiments were performed on a Bruker AVANCE AV 400 MHz spectrometer. All of the titration experiments were carried out at 25 °C in a 90% H2O/10% D_2O solution containing 150 mM KCl and 25 mM potassium phosphate buffer (pH 7.0). Water suppression was achieved by the Watergate method.[23,55] The oligonucleotide d(T$_2$AG$_3$) was purified by HPLC, and the concentration was 0.5 mM for the NMR measurements. For the thermal denature experiments, spectra were taken at intervals of 5 °C over the range 25−90 °C, with a constant temperature being maintained for 15 min prior to each reading to ensure a stable signal.

Molecular Modeling. The crystal structure of the parallel 22-mer telomeric G-quadruplex (PDB ID 1KF1)[48] was used as an initial model to study the interaction between the quindoline derivatives and telomeric DNA. The terminal 5′ adenine residue was removed to generate a 21-mer structure. Water molecules were removed from the PDB file, whereas the missing hydrogen atoms were added to the system using the Biopolymer module implemented in the SYBYL7.3.5 molecular modeling software from Tripos Inc. (St. Louis, MO). Ligand structures were constructed by adopting the empirical Gasteiger−Huckel (GH) partial atomic charges and then were optimized (Tripos force field) with a nonbond cutoff of 12 Å and a convergence of 0.01 kcal mol^{-1}/Å over 10000 steps using the Powell conjugate-gradient algorithm.

Docking studies were carried out using the AUTODOCK 4.0 program.[56] Using ADT,[57] nonpolar hydrogens of telomeric G-quadruplex was merged to their corresponding carbons and partial atomic charges were assigned. The nonpolar hydrogens of the ligands were merged, and rotatable bonds were assigned. The resulting G-quadruplex structure was used as an input for the AUTOGRID program. AUTOGRID performed a precalculated atomic affinity grid maps for each atom type in the ligand plus an electrostatics map and a separate desolvation map present in the substrate molecule. The dimensions of the active site box, which was placed at the center of the G-quadruplex, were set to 50 Å × 50 Å × 50 Å with the grid points 0.375 Å apart. Docking calculations were carried out using the Lamarckian genetic algorithm (LGA). Initially, we used a population of random individuals (population size: 150), a maximum number of 5000000 energy evaluations, a maximum number of generations of 27000, and a mutation rate of 0.02. One hundred independent docking runs were done for each ligand. The resulting positions were clustered according to a root-mean-square criterion of 0.5 Å.

Molecular dynamics simulations were performed with the FF99 version of the Cornell et al. force field[58] using the sander module of the Amber 10.0 program suite. The nucleic acids studied were as treated using the parm99 parameters. Partial atomic charges for the ligand molecules were calculated using Gasteiger method, while force-field parameters were taken from the generalized Amber force field (GAFF)[59] using ANTECHAMBER module. A formal positive charge was manually assigned to the ammonium group present in the side chain and the 5-position of aromatic core. The K^+ radius was kept at 2.025 Å.[60] Periodic boundary conditions were applied with the particle-mesh Ewald (PME) method[61] used to treat long-range electrostatic interactions. The quadruplex and ligand complexes were solvated in a rectangular box of TIP3P[62] water molecules with solvent layers 8 Å, and the potassium counterions were added to neutralize the complexes.

The hydrogen bonds were constrained using SHAKE.[63] For the nonbonded interactions, a residue-based cutoff of 10 Å was used. Temperature regulation was achieved by Langevin coupling with a collision frequency of 1.0. The solvated structures were subjected to initial minimization to equilibrate the solvent and counter cations. The G-quadruplex and inner K^+ ions were initially fixed with force constants of 100 kcal mol^{-1}. The system was then heated from 0 to 300 K in a 100 ps simulation and followed by a 100 ps simulation to equilibrate the density of the system. Afterward, constant pressure MD simulation of 1 ns was then performed in an NPT ensemble at 1 atm and 300 K. The output and trajectory files were saved every 0.1 and 1 ps for the subsequent analysis, respectively. All trajectory analysis was done with the Ptraj module in the Amber 10.0 suite and examined visually using the VMD software package.[64]

The MM/GBSA method[65] implemented in the AMBER 10.0 suite was used to calculate the binding free energy between the G-quadruplex and the quindoline derivatives. All the waters and counterions were stripped off but including the K^+ present within the negatively charged central channel. The set of 500 snapshots

from MD trajectories were collected to calculate the binding free energies. The formula was used as:

$$\Delta G = \Delta E_{MM} + \Delta G_{solv} + \Delta G_{np} - T\Delta S_{MM}$$

$$E_{MM} = E_{int} + E_{elstat} + E_{vdW}$$

E_{MM} is the internal molecular mechanics energy (comprises internal bonding energy terms, nonbonding electrostatic, and van der Waals interations), G_{solv} is the solvation free energy calculated by solving generalized Born[65] equations, G_{np} is the nonpolar part of the solvation free energy calculated from solvent-accessible surface area (SASA),[66] and $T\Delta S$ is the solute entropy, which is usually estimated by normal-mode analysis method.[67]

Competition Dialysis Experiment. Competition dialysis experiments were performed as previously described.[50] A Tris-HCl buffer (10 mM, pH 7.4) containing 100 mM NaCl was used for all experiments. For each competition dialysis assay, test ligands (1 mM concentration, 200 mL volume) were dialyzed against the nucleic acid array. A volume of 0.5 mL (at 45 μM monomeric unit) of each of the DNA samples was pipetted into a separate 0.5 mL Spectro/Por DispoDialyzer unit with a 1000 molecular weight cutoff tubing (Spectrum, Laguna Hills, CA). A panel of 10 different nucleic acid structures used was listed in Table 4. The entire dialysis units were then placed in the beaker containing the dialysate solution. At the end of the 24 h equilibration period at room temperature, DNA samples were carefully removed to microfuge tubes and were taken to a final concentration of 1% (w/v) sodium dodecyl sulfate (SDS). The total concentration of ligand (C_t) within each dialysis tube was then measured spectrophotometrically at 425 nm with an extinction coefficient of 10780 $M^{-1}\cdot cm^{-1}$ for **2b** and at 415 nm with an extinction coefficient of 11410 $M^{-1}\cdot cm^{-1}$ for **1**. The free ligand concentration (C_f) was determined spectrophotometrically using an aliquot of the dialysate solution. The amount of bound ligand was determined by the difference between the total ligand concentration and the free ligand concentration ($C_b = C_t - C_f$). Final analysis of the data was carried out using the Origin 7.5 software (OriginLab Corp.).

Cell-Free Telomerase Activity Assay. The ability of ligands to inhibit telomerase in a cell-free system was assessed with a modified TRAP using the extracts from exponentially growing MCF-7 breast carcinoma cells as described previously.[51] Briefly, the TRAP assay was carried out in two steps including telomerase-mediated primer-elongation and PCR amplification of the telomerase products to enable detection. PCR was performed in a final 50 μL reaction volume composed of a 45 μL reaction mix containing 20 mM Tris-HCl (pH 8.0), 50 μM dNTPs, 1.5 mM $MgCl_2$, 63 mM KCl, 1 mM EGTA, 0.005% Tween 20, 20 μg/mL BSA, 3.5 pmol of primer TSG4 d($G_3AT_2G_3AT_2G_3AT_2G_3T_2$), 18 pmol of primer TS d($A_2TC_2GTCGAGCAGAGT_2$), 22.5 pmol of primer CXext d($GTGC_3T_2AC_3T_2AC_3T_2AC_2CTA_2$), 7.5 pmol of primer NT d($ATCGCT_2CTCG_2C_2T_4$), 0.01 amol of TSNT internal control d($AT_2C_2GTCGAGCAGAGT_2A_3G_2C_2GAGA_2GCGAT$), 2.5 units of *Taq* DNA polymerase, and 100 ng of the extracts. Compounds or distilled water were added under a volume of 5 μL. PCR were performed in an Eppendorf Mastercycler equipped with a hot lid and incubated for 30 min at 30 °C, followed by 92 °C 30 s, 52 °C 30 s, and 72 °C 30 s for 30 cycles. After amplification, 8 μL of loading buffer (containing 5× Tris-Borate-EDTA buffer (TBE buffer), 0.2% bromphenol blue, and 0.2% xylene cyanol) were added to the reaction. A 15 μL aliquot was loaded onto a 10% nondenaturing acrylamide gel (19:1) in 1× TBE buffer and run at 200 V for 1 h. Gels were fixed and then stained with $AgNO_3$. $^{Tel}IC_{50}$ values were then calculated from the optical density with the LadWorks software.

Telomere Length Assay. To measure the telomere length, genomic DNA was digested with Hinf1/Rsa1 restriction enzymes. The digested DNA fragments were separated on 0.8% agarose gel, transferred to a nylon membrane, and the transferred DNA fixed on the wet blotting membrane by baking the membrane at 120 °C for 20 min. Membrane was hybridized with a DIG-labeled hybridization probe for telomeric repeats and incubated with anti-DIG-alkaline phosphatase. TRF was performed by chemiluminescence detection.

Short-Term Cell Viability. HL60 and CA46 cells were seeded on 96-well plates (1.0×10^3/well) and exposure to various concentrations of ligands. After 48 h of treatment at 37 °C in a humidified atmosphere of 5% CO_2, 10 μL of 5 mg/mL methyl thiazolyl tetrazolium (MTT) solution was added to each well and further incubated for 4 h. The cells in each well were then treated with dimethyl sulfoxide (DMSO) (200 μL for each well) and the optical density (OD) was recorded at 570 nm. All drug doses were parallel tested in triplicate, and the IC_{50} values were derived from the mean OD values of the triplicate tests versus drug concentration curves.

Long-Term Cell Culture Experiments. Long-term proliferation experiments were carried out using the HL60 leukemia cell line and CA46 lymphoma cell line. Cells were grown in T80 tissue culture flasks at 1.0×10^5 per flask and exposed to a subcytotoxic concentration of ligand or an equivalent volume of 0.1% DMSO every 4 days. The cells in control and drug-exposed flasks were counted and flasks reseeded with 1.0×10^5 cells. The remaining cells were collected and used for measurements described below. This process was continued for 16 days.

SA-β-Gal Assay.[21] Cells treated with the ligand were incubated for 16 days. After the incubation, the growth medium was aspirated and the cells were fixed in 2% formaldehyde/0.2% glutaraldehyde for 15 min at room temperature. The fixing solution was removed and the cells were gently washed twice with PBS and then stained using the β-Gal stain solution containing 1 mg/mL of 5-bromo-4-chloro-3-indolyl-β-D-galactoside, followed by incubation overnight at 37 °C. The staining solution was removed, and the cells were washed three times with PBS. The cells were viewed under an optical microscope and photographed.

Acknowledgment. We thank the National Nature Science Foundation of China (20472117 and 20772159), the NSFC/RGC Joint Research Scheme (30731160006 and N_PolyU 508/06), the Science Foundation of Guangzhou (2006Z2-E402), the Science Foundation of Zhuhai (grant PC20041131), the NCET, the Shenzhen Key Laboratory Fund, and the University Grants Committee Areas of Excellence Scheme in Hong Kong (AoE P/10-01) for financial support of this study. We also thank Dr. Hai-Bin Luo, School of Pharmaceutical Sciences in Sun Yat-sen University, for his assistance with the molecular modeling studies.

Note Added after ASAP Publication. This paper published ASAP on September 27, 2008 without the author affiliation information. The correct version was published on October 16, 2008.

Supporting Information Available: CD spectra of HTG21 with 5-*N*-methyl quindolines **2a**−**x** and nonmethylated quindolines, NMR spectra of [d(T2AG3)]$_4$ with ligand **2r**, molecular modeling studies, MS, and ^{1}H NMR spectra of compounds **3a**−**d** and **4a**−**d**, HRMS and ^{1}H and ^{13}C NMR spectra of compounds **2a**−**x**. This material is available free of charge via the Internet at http://pubs.acs.org.

References

(1) Blackburn, E. H. Structure and function of telomeres. *Nature* **1991**, *350*, 569–573.
(2) Blackburn, E. H. Switching and signaling at the telomere. *Cell* **2001**, *106*, 661–673.
(3) Harley, C. B.; Futcher, A. B.; Greider, C. W. Telomeres shorten during aging of human Fibroblasts. *Nature* **1990**, *345*, 458–460.
(4) Greider, C. W.; Blackburn, E. H. Identification of a specific telomere terminal transferase activity in *Tetrahymena* extracts. *Cell* **1985**, *43*, 405–413.
(5) Feng, J.; Funk, W.; Wang, S.-S.; Weinrich, S. L.; Avilion, A. A.; Chiu, C.-P.; Adam, R. R.; Chang, E. The RNA component of human telomerase. *Science* **1995**, *269*, 1236.

(6) Kim, N. W.; Piatyszek, M. A.; Prowse, K. R.; Harley, C. B.; West, M. D.; Ho, P. L.; Coviello, G. M.; Wright, W. E.; Weinrich, S. L.; Shay, J. W. Specific association of human telomerase activity with immortal cell and cancer. *Science* **1994**, *266*, 2011–2015.
(7) Bryan, T. M.; Cech, T. R. Telomerase and maintenance of chromosome ends. *Curr. Opin. Cell Biol.* **1999**, *11*, 318–322.
(8) Masutomi, K.; Yu, E. Y.; Khurts, S.; Ben-Porath, I.; Currier, J. L.; Metz, G. B.; Brooks, M. W.; Kaneko, S.; Murakami, S.; DeCaprio, J. A.; Weinberg, R. A.; Stewart, S. A.; Hahn, W. C. Telomerase maintains telomere structure in normal human cells. *Cell* **1999**, *114*, 241–253.
(9) Herbert, B. S.; Pitts, A. E.; Baker, S. I.; Hamilton, S. E.; Wright, W. E.; Shay, J. W.; Corey, D. R. Inhibition of human telomerase in immortal human cells leads to progressive telomere shortening and cell death. *Proc. Natl. Acad. Sci. U.S.A.* **1999**, *96*, 14276–14281.
(10) Neidle, S.; Parkinson, G. Telomere maintenance as a target for anticancer drug discovery. *Nat. Rev. Drug Discovery* **2002**, *1*, 383–393.
(11) Herbert, B. S.; Pitts, A. E.; Baker, S. I.; Hamilton, S. E.; Wright, W. E.; Shay, J. W.; Corey, D. R. Inhibition of human telomerase in immortal human cells leads to progressive telomere shortening and cell death. *Proc. Natl. Acad. Sci. U.S.A.* **1999**, *96*, 14276–14281.
(12) Mergny, J.-L.; Riou, J.-F.; Mailliet, P.; Teulade-Fichou, M.-P.; Gilson, E. Natural and pharmacological regulation of telomerase. *Nucleic Acids Res.* **2002**, *30*, 839–865.
(13) Rezler, E. M.; Rearss, D. J.; Hurley, L. H. Telomeres and telomerases as drug targets. *Curr. Opin. Pharmacol.* **2002**, *2*, 415–423.
(14) De Cian, A.; Lacroix, L.; Douarre, C.; Temime-Smaali, N.; Trentesaux, C.; Riou, J.-F.; Mergny, J.-L. Targeting telomeres and telomerase. *Biochime* **2008**, *90*, 131–155.
(15) Ou, T.-M.; Lu, Y.-J.; Tan, J.-H.; Huang, Z.-S.; Wong, K.-Y.; Gu, L.-Q. G-quadruplexes: targets in anticancer drug design *ChemMedChem* **2008**, DOI:10.1002/cmdc.200700300.
(16) Neidle, S.; Parkinson, G. N. The structure of telomeric DNA. *Curr. Opin. Struct. Biol.* **2003**, *13*, 275–283.
(17) Kim, M.-Y.; Vankayalapati, H.; Shin-ya, K.; Wierzba, K.; Hurley, L. H. Telomestatin, a Potent Telomerase Inhibitor That Interacts Quite Specifically with the Human Telomeric Intramolecular G-Quadruplex. *J. Am. Chem. Soc.* **2002**, *124*, 2098–2099.
(18) Wheelhouse, R. T.; Sun, D.; Han, H.; Han, F. X.; Hurley, L. H. Cationic Porphyrins as Telomerase Inhibitors: the Interaction of Tetra(*N*-methyl-4-pyridyl)porphine with Quadruplex DNA. *J. Am. Chem. Soc.* **1998**, *120*, 3261–3262.
(19) Read, M. A.; Wood, A. A.; Harrison, J. R.; Gowan, S. M.; Kelland, L. R.; Dosanjh, H. S.; Neidle, S. Molecular Modeling Studies on G-Quadruplex Complexes of Telomerase Inhibitors: Structure−Activity Relationships. *J. Med. Chem.* **1999**, *42*, 4538–4546.
(20) Read, M.; Harrison, R. J.; Romagnoli, B.; Tanious, F. A.; Gowan, S. H.; Reszka, A. P.; Wilson, W. D.; Kelland, L. R.; Neidle, S. Structure-based design of selective and potent G quadruplex-mediated telomerase inhibitors. *Proc. Natl. Acad. Sci. U.S.A.* **2001**, *98*, 4844–4849.
(21) Moore, M. J. B.; Schultes, C. M.; Cuesta, J.; Cuenca, F.; Gunaratnam, M.; Tanious, F. A.; Wilson, W. D.; Neidle, S. Trisubstituted acridines as G-quadruplex telomere targeting agents. Effects of extensions of the 3,6- and 9- side chains on quadruplex binding, telomerase activity, and cell proliferation. *J. Med. Chem.* **2006**, *49*, 582–599.
(22) Cookson, J. C.; Heald, R. A.; Stevens, M. F. G. Antitumor polycyclic acridines. 17. Synthesis and pharmaceutical profiles of pentacyclic acridinium salts designed to destabilize telomeric integrity. *J. Med. Chem.* **2005**, *48*, 7198–7207.
(23) Fedoroff, O. Y.; Salazar, M.; Han, H.; Chemeris, V. V.; Kerwin, S. M.; Hurley, L. H. NMR-based model of a telomerase-inhibiting compound bound to G-quadruplex DNA. *Biochemistry* **1998**, *37*, 12367–12374.
(24) Kern, J. T.; Wang, T. P.; Kerwin, S. M. The relationship between ligand aggregation and G-quadruplex DNA selectivity in a series of 3,4,9,10-perylenetetracarboxylic acid diimides. *Biochemistry* **2002**, *41*, 11379–11389.
(25) Gomez, D.; Aouali, N.; Renaud, A.; Douarre, C.; Shin-ya, K.; Tazi, J.; Martinez, S.; Trentesaux, C.; Morjani, H.; Riou, J.-F. Resistance to senescence induction and telomere shortening by a G-quadruplex ligand inhibitor of telomerase. *Cancer Res.* **2003**, *63*, 6149–6153.
(26) Izbicka, E.; Wheelhouse, R. T.; Raymond, E.; Davidson, K. K.; Lawrence, R. A.; Sun, D.; Windle, B. E.; Hurley, L. H.; Von Hoff, D. D. Effects of cationic porphyrins as G-quadruplex interactive agents in human tumor cells. *Cancer Res.* **1999**, *59*, 639–644.
(27) Missailidis, S.; Stanslas, J.; Modi, C.; Ellis, M. J.; Robins, R. A.; Laughton, C. A.; Stevens, M. F. G. Antitumor polycyclic acridines. Part 12. Physical and biological properties of 8,13-diethyl-6-methylquino[4,3,2-*kl*]acridinium iodide: a lead compound in anticancer drug design. *Oncol. Res.* **2002**, *13*, 175–189.
(28) Gowan, S. M.; Heald, R.; Stevens, M. F. G.; Kelland, L. R. Potent inhibition of telomerase by small-molecule pentacyclic acridines capable of interacting with G-quadruplexes. *Mol. Pharmacol.* **2001**, *60*, 981–988.
(29) Holt, S. J.; Petrow, V. Cabarzole, carbolines, and related compounds [Part 1]. *J. Chem. Soc.* **1947**, 607–611.
(30) Bierer, D. E.; Dubenko, L. G.; Zhang, P. Antihyperglycemic activities of cryptolepine analogues: an ethnobotanical lead structure from *Cryptolepis sanguinolenta*. *J. Med. Chem.* **1998**, *41*, 2754–2764.
(31) Yang, S.-W.; Abdel-Kader, M.; Malone, S.; Werkhoven, M. C.; Wisse, J. H.; Bursuker, I.; Neddermann, K.; Fairchild, C.; Raventos-Suarez, C.; Menendez, A. T.; Lane, K.; Kingston, D. G. Synthesis and biological evaluation of analogues of cryptolepine, an alkaloid isolated from Suriname Rainforest. *J. Nat.Prod* **1999**, *62*, 976–983.
(32) Lisgarten, J. N.; Coll, M.; Portugal, J. W. W. C.; Aymami, J. The antimalaral and cytotoxic drug cryptolepine intercalates into DNA at cytosine−cytosine sites. *Nat. Struct. Biol.* **2002**, *9*, 57–60.
(33) Caprio, V.; Guyen, B.; Opoku-Boahen, Y.; Mann, J.; Gowan, S. M.; Kelland, L. M.; Read, M. A.; Neidle, S. A novel inhibitor of human telomerase derived from 10*H*-indolo-[3,2-*b*]quinoline. *Bioorg. Med. Chem. Lett.* **2000**, *10*, 2063–2066.
(34) Guyen, B.; Schultes, C. M.; Hazel, P.; Mann, J.; Neidle, S. Synthesis and evaluation of analogs of 10*H*-indolo[3,2-*b*]quinoline as G-quadruplex stabilizing ligands and potential inhibitors of the enzyme telomerase. *Org. Biomol. Chem.* **2004**, *2*, 981–988.
(35) LeSanna, C.; Huddlestona, J.; Mann, J. Synthesis and preliminary evaluation of novel analogues of quindolines as potential stabilisers of telomeric G-quadruplex DNA. *Tetrahedron* **2007**, *63*, 12903–12911.
(36) Zhou, J.-L.; Lu, Y.-J.; Ou, T.-M.; Zhou, J.-M.; Huang, Z.-S.; Zhu, X.-F.; Du, C.-J.; Bu, X.-Z.; Ma, L.; Gu, L.-Q.; Li, Y.-M.; Chan, A. S.-C. Synthesis and evaluation of quindoline derivatives as G-quadruplex inducing and stabilizing ligands and potential inhibitors of telomerase. *J. Med. Chem.* **2005**, *48*, 7315–7321.
(37) Zhou, J. M.; Zhu, X. F.; Lu, Y. J.; Deng, R.; Huang, Z. S.; Mei, Y. P.; Wang, Y.; Huang, W. L.; Liu, Z. C.; Gu, L. Q.; Zeng, Y. X. Senescence and telomere shortening induced by novel potent G-quadruplex interactive agents, quindoline derivatives, in human cancer cell lines. *Oncogene* **2006**, *25*, 503–511.
(38) Monchaud, D.; Teulade-Fichou, M. P. A hitchhiker's guide to G-quadruplex ligands. *Org. Biomol. Chem.* **2008**, *6*, 627–636.
(39) Fan, P.; Ablordeppey, S. Y. An alternative synthesis of 10*H*-Indolo[3,2-*b*]quinoline and its selective *N*-alkylation. *J. Heterocycl. Chem.* **1997**, *34*, 1789–1794.
(40) Li, W.; Wu, P.; Ohmichi, T.; Sugimoto, N. Characterization and thermodynamic properties of quadruplex/duplex competition. *FEBS Lett.* **2002**, *526*, 77–81.
(41) Balagurumoorthy, P.; Brahmachari, S. K.; Mohanty, D.; Bansal, M.; Sasisekharan, V. Hairpin and parallel quartet structures for telomeric sequences. *Nucleic Acids Res.* **1992**, *20*, 4061–4067.
(42) Rezler, E. M.; Seenisamy, J.; Bashyam, S.; Kim, M.-Y.; White, E.; Wilson, W. D.; Hurley, L. H. Telomestatin and diseleno sapphyrin bind selectively to two different forms of the human telomeric G-quadruplex structure. *J. Am. Chem. Soc.* **2005**, *127*, 9439–9447.
(43) Paramasivan, S.; Rujan, I.; Bolton, P. H. Circular dichroism of quadruplex DNAs: applications to structure, cation effects and ligand binding. *Methods* **2007**, *43*, 324–331.
(44) Mergny, J.-L.; Lacroix, L.; Teulade-Fichou, M.-P.; Hounsou, C.; Guittat, L.; Hoarau, M.; Arimondo, P. B.; Vigneron, J.-P.; Lehn J.-M.; Riou, J.-F.; Garestier, T.; Helene, C. Telomerase inhibitors based on quadruplex ligands selected by a fluorescence assay. *Proc. Natl. Acad. Sci. U.S.A.* **2001**, *98*, 3062–3067.
(45) De Cian, A.; Guittat, L.; Kaiser, M.; Sacca, B.; Amrane, S.; Bourdoncle, A.; Alberti, P.; Teulade-Fichou, M. P.; Lacroix, L.; Mergny, J. L. Fluorescence-based melting assays for studying quadruplex ligands. *Methods* **2007**, *42*, 183–95.
(46) Han, H.; Hurley, L. H.; Salazar, M. A DNA polymerase stop assay for G-quadruplex-interactive compounds. *Nucleic Acids Res.* **1999**, *27*, 537–542.
(47) Lemarteleur, T.; Gomez, D.; Paterski, R.; Mandine, E.; Mailliet, P.; Riou, J.-F. Stabilization of the c-myc gene promoter quadruplex by specific ligands' inhibitors of telomerase. *Biochem. Biophys. Res. Commun.* **2004**, *323*, 802–808.
(48) Parkinson, G. N.; Lee, M. P. H.; Neidle, S. Crystal structure of parallel quadruplexes from human telomeric DNA. *Nature* **2002**, *417*, 876–880.
(49) Bates, P.; Mergny, J. L; Yang, D. Quartets in G-major. *EMBO Rep.* **2007**, *8*, 1003–1010.
(50) Ragazzon, P.; Chaires, J. B. Use of competition dialysis in the discovery of G-quadruplex selective ligands. *Methods* **2007**, *43*, 313–323.
(51) Gomez, D.; Mergny, J.-L.; Riou, J.-F. Detection of telomerase inhibitors based on G-quadruplex ligands by a modified telomeric repeat amplification protocol assay. *Cancer Res.* **2002**, *62*, 3365–3368.

(52) De Cian, A.; Cristofari, G.; Reichenbach, P.; De Lemos, E.; Monchaud, D.; Teulade-Fichou, M.-P.; Shin-ya, K.; Lacroix, L.; Lingner, J.; Mergny, J.-L. Reevaluation of telomerase inhibition by quadruplex ligands and their mechanisms of action. *Proc. Natl. Acad. Sci. USA* **2007**, *104*, 17347–17352.

(53) Hwang, E. S. Replicative senescence and senescence-like state induced in cancer-derived cells. *Mech. Aging Dev.* **2002**, *123*, 1681–1694.

(54) Roninson, I. B. Tumor senescence as a determinant of drug response in vivo. *Drug Resist. Updates* **2002**, *5*, 204–208.

(55) Mita, H.; Ohyama, T.; Tanaka, Y.; Yamamoto, Y. Formation of a complex of 5,10,15,20-tetrakis(*N*-methyl-pyridinium-4-yl)-21*H*,23*H*-porphyrin with G-quadruplex DNA. *Biochemistry* **2006**, *45*, 6765–6772.

(56) Morris, G. M.; Goodsell, D. S.; Halliday, R. S.; Huey, R.; Hart, W. E.; Belew, R. K.; Olson, A. J. Automated docking using a Lamarckian genetic algorithm and an empirical binding free energy function. *J. Comput. Chem.* **1998**, *19*, 1639–1662.

(57) Sanner, M. F. Python: a programming language for software integration and development. *J. Mol. Graphics Modell.* **1999**, *17*, 57–61.

(58) Cornell, W. D.; Cieplak, C. I.; Bayly, I. R.; Gould, I. R.; Merz, K. M.; Ferguson, D. M.; Spellmeyer, D. C.; Fox, T.; Caldwell, J. W.; Kollman, P. A. A second generation force field for the simulation of proteins, nucleic acids and organic molecules. *J. Am. Chem. Soc.* **1995**, *117*, 5179–5197.

(59) Wang, J.; Wolf, R. M.; Caldwell, J. W.; Kollman, P. A.; Case, D. A. Development and testing of a general amber force field. *J. Comput. Chem.* **2004**, *25*, 1157–1174.

(60) Hazel, P.; Parkinson, G. N.; Neidle, S. Predictive modelling of topology and loop variations in dimeric DNA quadruplex structures. *Nucleic Acids Res.* **2006**, *34*, 21172127.

(61) Darden, T.; York, D.; Pedersen, L. Particle mesh Ewald: An *N* log−(*N*) method for Ewald sums in large systems. *J. Chem. Phys.* **1993**, *98*, 10089–10092.

(62) Jorgensen, W. L.; Chandrasekhar, J.; Madura, J. D.; Impey, R. W.; Klein, M. L. Comparison of simple potential functions for simulating liquid water. *J. Chem. Phys.* **1983**, *79*, 926–935.

(63) Ryckaert, J. P.; Ciccotti, G.; Berendsen, H. J. C. Numerical integration of the cartesian equations of motion of a system with constraints: molecular dynamics of *n*-alkanes. *J. Comput. Phys.* **1977**, *23*, 327–341.

(64) Humphrey, W.; Dalke, A.; Schulten, K. VMD: visual molecular dynamics. *J. Mol. Graphics* **1996**, *14*, 33–38.

(65) Kollman, P. A.; Massova, I.; Reyes, C.; Kuhn, B.; Huo, S. H.; Chong, L.; Lee, M.; Lee, T.; Duan, Y.; Wang, W.; Donini, O.; Cieplak, P.; Srinivasan, J.; Case, D. A.; Cheatham, T. E. Calculating structures and free energies of complex molecules: combining molecular mechanics and continuum models. *Acc. Chem. Res.* **2000**, *33*, 889–897.

(66) Sitkoff, D.; Sharp, K. A.; Honig, B. Accurate calculation of hydration free energies using macroscopic solvent models. *J. Phys. Chem.* **1994**, *98*, 1978–1988.

(67) Kottalam, J.; Case, D. A. Langevin modes of macromolecules—applications to Crambin and DNA hexamers. *Biopolymers* **1990**, *29*, 1409–1421.

JM800497P